Ground-Based Polarimetric SAR Interferometry for the Monitoring of Terrain Displacement Phenomena. Part II: Applications

Rubén Iglesias, *Student Member, IEEE*, Albert Aguasca, *Member, IEEE*, Xavier Fabregas, *Member, IEEE*, Jordi J. Mallorqui, *Senior Member, IEEE*, Dani Monells, *Student Member, IEEE*, Carlos López-Martínez, *Senior Member, IEEE*, and Luca Pipia

***Abstract*—Urban subsidence and landslides are among the greatest hazards for people and infrastructure safety and they require an especial attention to reduce their associated risks. In this framework, ground-based synthetic aperture radar (SAR) interferometry (GB-InSAR) represents a cost-effective solution for the precise monitoring of displacements. This work presents the application of GB-InSAR techniques, particularly with the RiskSAR sensor and its processing chain developed by the Remote Sensing Laboratory (RSLab) of the Universitat Politècnica de Catalunya (UPC), for the monitoring of two different types of ground displacement. An example of urban subsidence monitoring over the village of *Sallent*, northeastern of Spain, and an example of landslide monitoring in *El Forn de Canillo*, located in the Andorran Pyrenees, are presented. In this framework, the key processing particularities for each case are deeply analyzed and discussed. The linear displacement maps and time series for both scenarios are showed and compared with in-field data. For the study, fully polarimetric data acquired at X-band with a zero-baseline configuration are employed in both scenarios. The displacement results obtained demonstrate the capabilities of GB-SAR sensors for the precise monitoring of ground displacement phenomena.**

***Index Terms*—Differential synthetic aperture radar (SAR) interferometry (DInSAR), displacement monitoring, ground-based SAR (GB-SAR), frequency modulated continuous wave (FMCW) radar, ground-based SAR interferometry (GBInSAR), persistent scatterer interferometry (PSI), polarimetric SAR interferometry (PolInSAR), steepest linear frequency modulated continuous wave (SLFMCW) radar.**

I. Introduction

THE DEVELOPMENT of differential synthetic aperture radar (SAR) interferometry (DInSAR) algorithms during the last decade has demonstrated their usefulness for the precise monitoring of ground displacement episodes [1], [2] with millimetric precisions [3]. Furthermore, DInSAR algorithms have boosted the development of persistent scatterer interferometry (PSI) techniques which allows obtaining not only accurate linear velocity estimations but also time series containing the nonlinear displacement component of affected areas [4]–[15].

In this context, two different kinds of sensors may be considered: orbital/airborne or ground-based. Spaceborne SAR sensors have demonstrated to be extremely successful for studying the evolution of displacement processes, especially, over wide areas. Despite this, when flexibility in terms of revisiting time or sensor orientation toward the scene is required, orbital sensors cannot fulfill the requirements. Airborne sensors represent a more flexible solution but contrarily the data processing becomes more difficult. Furthermore, the monitoring campaigns are generally costly and complex to carry out. For this reason, the research activity of several groups has been recently addressed to the development of terrestrial SAR systems [16], [17]. Flexible, easy to deploy, and cheaper if compared to space- or airborne solutions, Ground-Based SAR (GB-SAR) sensors can be presented as an effective, and sometimes complementary, solution for the precise monitoring of small-scale phenomena [18]–[33].

Due to the capability of GB-SAR sensors to carry out a *quasi* continuous monitoring, one of their most relevant application corresponds to the slope monitoring of open pit mines, in which such systems potentially work as an Early Warning System (EWS) [34]–[37]. Other relevant applications include slope instability monitoring related to rock-slides [38], [39], [21], volcanoes [40], urban monitoring [41]–[43], structure monitoring [44], [16], dike monitoring [45], glacier monitoring [46], and landslides [43], [45], [47]–[50]. A complete classification of the different GB-SAR applications can be found in [51].

This paper presents the applicability of the RiskSAR GB-SAR sensor, developed in the Remote Sensing Laboratory (RSLab) of the Universitat Politècnica de Catalunya (UPC) and widely described in Part I of this paper [52], for the efficient monitoring of ground displacement phenomena.

The RiskSAR sensor [22], [29] is based on the employment of high-rate steepest linear frequency modulated continuous wave (SLFMCW) signals. This type of solution allows performing faster scans compared with vector network analyzer (VNA)-based solutions and, hence, minimize the impact of

Manuscript received March 31, 2014; revised July 22, 2014; accepted September 18, 2014. This work was supported in part by the Big Risk Project (contract number BIA2008-06614), and in part by the Project TEC2011-28201-C02-01 funded by the Spanish MICINN and FEDER funds.

R. Iglesias, A. Aguasca, X. Fabegas, J. J. Mallorqui, D. Monells, and C. López-Martínez are with the Department of Signal Theory and Communications, Universitat Politècnica de Catalunya, 08034 Barcelona, Spain (e-mail: ruben.iglesias@tsc.upc.edu; aguasca@tsc.upc.edu; fabregas@tsc.upc.edu; mallorqui@tsc.upc.edu; dmonells@tsc.upc.edu; carlos.lopez@tsc.upc.edu).

L. Pipia is with the Institut Cartogràfic Geològic de Catalunya, 08038 Barcelona, Spain (e-mail: luca.pipia@icc.cat).

Color versions of one or more of the figures in this paper are available online at http://ieeexplore.ieee.org.

Digital Object Identifier 10.1109/JSTARS.2014.2366711

tropospheric disturbances and target instabilities during the scanning time. This radar architecture also favors obtaining reliable polarimetric SAR (PolSAR) measurements with no dramatic increase in the scanning time. In this context, it has been recently demonstrated that polarimetric SAR interferometry (PolInSAR) techniques outperform classical single-polarization PSI performance [53]–[55].

The applications shown in this work are focused on the GB-SAR sensor working in a discontinuous operation mode, which means revisiting the site during different measurement days with a certain temporal span. This can be applied when the deformation process is slow enough and does not require a continuous monitoring. As widely explained in [52], the processing for this configuration mode consists of performing first a temporal averaging of each daily data set. This is referred to as short-term processing (STP) and allows improving the signal-to-noise ratio (SNR) of time-stationary targets, leading to a time-averaged SLC image for each measurement day. In the following step, referred to as long-term processing (LTP), the atmospheric artifacts among the different time-averaged SLC images are compensated for. From all methods available in the literature, the RiskSAR processing chain makes use of model-based solutions to carry out the atmospheric phase screen (APS) compensation. This kind of solution has proven to be very effective since it reaches very good results with no need of extra meteorological data or stable ground control points (GCP). Carrying out a proper APS estimation and compensation process is mandatory in order to obtain reliable displacement map estimations. Once a set of APS-free interferograms are obtained, PSI techniques can be applied to obtain reliable linear and nonlinear estimations of ground displacements. Among all the PSI techniques developed in the last decade, this work focuses on the adaptation of the coherent pixels technique (CPT) to work with zero-baseline data [52].

The linear displacement maps and time series over two very different scenarios, a district affected by subsidence due to the mining activity carried out in the surrounding area during the last century, and an active slow-moving landslide located in a mountainous region, are presented. The main logistics and processing particularities for each case are widely discussed. In both scenarios, the RiskSAR sensor was operated at X-band due to its excellent tradeoff among the high spatial resolution of the SLC images acquired, the possibility to achieve a reliable APS compensation and a fine sensitivity to ground displacements. For this reason, the RiskSAR sensor is referred to as RiskSAR-X hereinafter. The slant-range resolution working at X-band is 1.25 m. The cross-range resolution is on the order of 10 mrad, ranging from 0.75 m at near range up to roughly 5 m at a far range of 1500 m. In both cases, the processing is benefited from the use of fully polarimetric data.

The paper is organized as follows. Section II refers to GB-SAR measurement logistics, with emphasis in the importance of choosing a correct location for the sensor depending on the nature of the scenario and on the ground displacement process characteristics. Sections III and IV present the zero-baseline PSI results in the urban scenario of *Sallent* and in the landslide of *El Forn de Canillo*, respectively. The main conclusion and major remarks are given in Section V.

II. Measurement Logistics

Once a GB-SAR solution is adopted for the monitoring of a certain area, the location of the sensor constitutes a crucial issue in order to maximize the performance of the technique. In addition to be able to cover the whole area of interest, two important aspects must be taken into account: the minimization of the so-called SAR geometrical distortions (foreshortening, layover, or shadowing) to have the regions of interest visible to the radar, and the maximization of the sensor sensitivity to deformation, as SAR systems are only able of detecting displacements in the line-of-sight (LOS) direction. The selection of the adequate emplacement helps to maximize the sensitivity of the interferometric phase to the deformation process to monitor, and thus provide the best results possible.

These aspects must be taken into account when planning the measurements and, furthermore, in the final interpretation of the results. This section presents their analysis in order to maximize the performance of ground-based SAR interferometry (GB-InSAR) techniques depending on the nature and environmental conditions of the displacement phenomenon.

A. Minimization of SAR Geometric Distortion Effects

Regardless of the platform nature, three geometric distortions are present in SAR imaging. These are the foreshortening, the layover, and the shadowing [56]. Unlike orbital-based SAR sensors, which are constrained by the orbit geometry, GB-SAR sensors allow fitting the sensor location and orientation to the specific characteristics of the area under study. This fact allows to minimize, or at least control, these distortion effects.

Shadowing must be especially taken into account when facing urban monitoring applications. Urbanized areas are typically characterized by having a relatively large number of tall man-made structures, such as buildings. If the location of the sensor is decided without considering its impact, it can lead to a large number of shaded areas in the SAR acquisitions. The location of the instrument at a certain height in order to achieve a top view of the area under study minimizes shadowing impact.

Contrarily, landslide areas are typically characterized by having a low numbers of man-made structures. Therefore, shadowing has less impact in these applications. Despite this, it is important to choose a location which allows overcoming the geographical accidents of the scenario. In these areas, foreshortening plays a more critical role. The illumination angle must depart from the local slope to avoid as much as possible the compression effect produced by this geometrical distortion. A good strategy consists of locating the instrument at the base of the hillside, some meters away from the slope, in order to illuminate all the area of interest minimizing the shadowing and the foreshortening artifacts.

B. Maximization of the Sensitivity to Deformation

As stated above, SAR systems only have sensitivity in the LOS direction. Due to its different orientation, the measured

displacements are, in general, not the real ones but a projection of them. Using a vector notation, both can be defined as

$$\mathbf{V}_{LOS} = |\mathbf{V_{LOS}}| \cdot \widehat{\mathbf{l}}_{\mathbf{LOS}}$$
$$\mathbf{V}_{G} = |\mathbf{V_G}| \cdot \widehat{\mathbf{l}}_{\mathbf{G}} \quad (1)$$

where $\mathbf{V}_G$ is the ground displacement vector, this is the real deformation, and $\mathbf{V}_{LOS}$ is the LOS displacement vector, this is the projection. The magnitudes $|\mathbf{V_{LOS}}|$ and $|\mathbf{V_G}|$ are related to the intensity of the displacement, and the unitary vectors $\widehat{\mathbf{l}}_{\mathbf{LOS}}$ and $\widehat{\mathbf{l}}_{\mathbf{G}}$ indicate the displacement direction. In fact, the former is only a projection of the latter. Thus, the magnitude of both displacement vectors can be related through a scalar product as follows:

$$|\mathbf{V_{LOS}}| = |\mathbf{V_G}| \cdot \cos(\alpha) \quad (2)$$

where

$$\cos(\alpha) = \widehat{\mathbf{l}}_{\mathbf{LOS}} \cdot \widehat{\mathbf{l}}_{\mathbf{G}} \quad (3)$$

being α the angle between the unitary vectors.

When the ground displacement is expected to be vertical, as it normally occurs with subsidence phenomena in urban scenarios, α directly becomes the local incidence angle θ_{inc}. In this context, higher sensor location elevations over the area of interest imply shorter incidence angles and thus a better sensitivity to the ground displacement.

When facing landslide monitoring the problem becomes more complex as the real motion of a particular point has an intrinsic topographic dependence related with its local slope. With no *a priori* knowledge, the more realistic kinetic model of the displacement direction $\widehat{\mathbf{l}}_{\mathbf{G}}$ is based on considering that the surface mostly moves along the steepest gradient of the terrain slope. This information may be derived employing a digital elevation model (DEM) of the area. Then, the angle α is directly obtained through (3).

For the current polar-orbiting SAR satellites, the look direction is close to East or West, for ascending or descending orbits, respectively. For this reason, spaceborne SAR systems are mainly sensitive to movements along slopes facing either East or West and almost insensitive to movements in North or South directions. In this context, GB-SAR sensors present a potential advantage with respect to spaceborne ones since they are not constrained by any orbit geometry. GB-SAR sensors can be placed at an adequate location and fit their orientation for illuminating a specific site according to the geometry of the problem.

A good strategy in landslide monitoring applications consists of locating the instrument at the foot of the hillside, using an illumination angle facing the down-slope direction in order to maximize the displacement detection.

III. Urban Monitoring Study Case

Urban monitoring represents one of the most interesting issues and major research topics in the SAR community. Subsidence hazards in urban areas involve from damage in man-made structures to the sudden collapse of entire neighborhoods, thus endangering human lives. Two surveying methods are mainly used for ground deformation monitoring purposes over urban scenarios. These are leveling and global positioning system (GPS). In most cases, the difficulty to cover large areas and the poor densities of measurements provided by these techniques hinder the effective identification and characterization of complex deformation episodes. Geotechnical devices such as inclinometers, extensometers, or piezometers present similar drawbacks.

GB-SAR sensors hence represent a useful alternative with respect to the previous surveying techniques. They provide precise estimations of ground displacement phenomena over larger areas with a high density of measures at a lower cost.

This section presents the study case of a linear urban subsidence phenomenon produced in a district affected by the former mining activity carried out around the area.

A. Test Site and Data Set

The test site selected corresponds to a district known as *El Barri de l'Estació*, located in the village of *Sallent*, northeastern Spain. Nowadays, there is a subsidence phenomenon induced by the intense mining activity carried out in the area during the second quarter of the last century. This deformation process is the consequence of the exploitation of the *Enrique Mine*, which was opened from 1932 to 1973 and reached a maximum depth of 260 m.

Unexpectedly, during the intense mining works of 1954, a natural cavity of about 120 m high and 40 m wide was found. Some years later, during 1957 and 1962, several floods from the *Llobregat River* occurred that made difficult to continue with the mine exploitation, and finally leading to the closure of the *Enrique Mine* in the year 1973.

During the period of abandoning, the mine was filled up with saturated salty water. Some decades after, in 1990s, heavy damages started to be appreciated in several man-made structures built within the affected district of *El Barri de l'Estació* [see Fig. 1(a)].

As a response to the problem, the administration started a research program to identify, characterize, and model the subsidence phenomena observed in the affected area [57]. A multiple set of techniques such as laser topographic leveling, geological mapping, geophysical prospection, extensometric measurements, and drilling was employed to evaluate the risk of the already weakened structures to collapse.

In this framework, the RSLab group, jointly with the Institut Cartogràfic i Geològic de Catalunya (ICGC), started in 2003, the study of this area with PSI techniques using spaceborne acquisitions of the European Remote Sensing (ERS) satellite [58]. A new collaboration between the RSLab and the ICGC started in 2006 to assess the performance of GB-SAR sensors in such scenarios. A 1-year measurement campaign was carried out using the RiskSAR-X sensor [22], [29]. It started in June 2006 and finished in March 2007. GB-SAR data were acquired during nine measurement days, as reported in Table I. In each measurement day, several scans were carried out in order to improve the SNR of measures.

(a) (b) (c)

F1:1 Fig. 1. (a) Example of the heavy damages observed in *El Barri de l'Estació*, *Sallent*. (b) Picture of the *El Barri de l'Estació* observed from the (c) RiskSAR point
F1:2 of view.

T1:1 TABLE I
T1:2 TIMETABLE OF SALLENT MEASUREMENT DAYS

Campaign	Date dd/mm/yyyy	Start Time hh:mm	Stop Time hh:mm	Numb. of Scans
1	29/06/2006	11:00	16:00	27
2	26/07/2006	08:00	11:30	30
3	19/08/2006	10:40	16:00	39
4	20/10/2006	09:40	15:00	31
5	14/11/2006	12:30	16:30	41
6	28/11/2006	19:00	08:40	44
7	18/12/2006	20:45	05:00	49
8	13/02/2007	22:00	09:55	37
9	14/03/2007	20:00	09:50	41

B. System Setup

As seen in Section II, in urban monitoring applications, the GB-SAR location must minimize as far as possible the effects produced by the buildings present in the scenario. This implies to select an emplacement as high as possible in order to have a top view of the area of interest, which minimizes the shadowing and maximizes the sensitivity to vertical displacements.

For these reasons, the instrument was finally installed on the top of a cliff of 84 m height, 200 m away in the range direction from the district *El Barri de l'Estació*. This location provided an incidence angle varying from 72° up to 82°. It is worth pointing out that installing the radar on the cliff's border prevented the radar front-end of saturations caused by close targets. Moreover, the system was placed on a base at approximately 30 cm above the ground to raise the rail and reduce the impact of the nearby vegetation.

Another important issue was to ensure a millimetric repositioning of the instrument to avoid a later coregistration of the data. In order to guarantee the repeatability of the observation conditions, the system was mounted over a cement base reinforced with a lightweight metallic frame. A picture of the RiskSAR-X point of view, and the final system setup is detailed in Fig. 1(b) and (c), respectively.

The area of interest illuminated by the RiskSAR sensor extended to approximately 400 m in range and 300 m in width. Each scan took roughly 2.5 min to perform a fully polarimetric measure.

C. Short-Term and Long-Term Processing

Prior to the application of the zero-baseline CPT algorithm to obtain PSI results, some important aspects about the STP and LTP [52] processing should be briefly remarked.

As seen, *El Barri de l'Estació* is an urban area plenty of man-made structures. For this reason, the reflectivity image of the region covered by the sensor has a large dynamic range, with strong reflectivity peaks corresponding to man-made structures, see Fig. 2(a). The coherence in these scenarios remains very high along the temporal axis, as illustrated in Fig. 2(b) and (c), which shows the coherence maps from two acquisitions with a temporal baseline of 15 min and 23 days, respectively. As shown, the highest coherence pixels are preserved in those areas with higher reflectivity, coinciding with the man-made structures present in the scenario. This fact is of crucial importance, since it will lead to a robust network of temporally coherent scatterers in the later PSI processing.

As it is detailed in [52], in addition to the thermal noise and the temporal decorrelation phenomena, APS represents the most relevant distortion artifact on the interferometric phase. It directly impacts in the STP, which aims to obtain a reliable high-quality time-averaged image from each measurement day. In addition, it also affects the LTP, whose objective is obtaining a collection of APS-free interferograms for the later PSI processing. From all the available methods, the RiskSAR sensor makes use of model-based solutions [59], [60] since they proved to be very successful with no extra meteorological data or stable GCP.

Fig. 2(d)–(f) shows the interferometric phase evolution due to APS between images separated by temporal spans of 15 min, 1 h, and 4 h, respectively. In such regions, the atmospheric artifacts are smooth in both the spatial and temporal domains. The linear approximation proposed in [59] is sufficient to deal with the APS problematic in these scenarios with soft topography [52].

In order to illustrate the good performance of APS model-based solutions in urban scenarios, the compensation process of an interferogram with a temporal span of 2 h is presented in Fig. 3. With the goal of generating a reliable vector of observations to carry out the linear regression, only the points with the highest coherence values ($\gamma > 0.95$) are employed. In order to estimate the coherence a 9×9 multilook is selected. Black dots represent the projection onto the range axis of the interferometric phase. Notice how, as expected, the interferometric phase

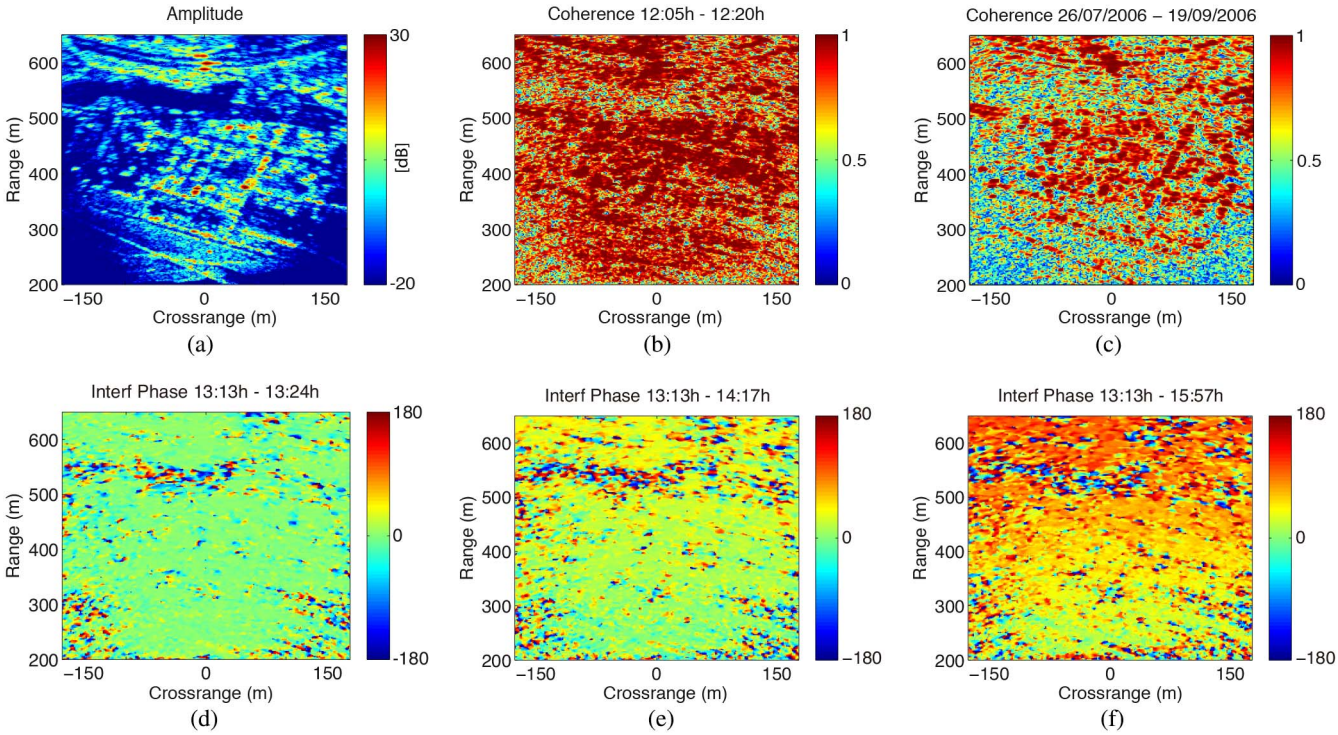

F2:1 Fig. 2. (a) Reflectivity image in dB and coherence maps between acquisitions with a temporal baseline of (b) 15 min and (c) 23 days corresponding to the area of
F2:2 *El Barri de l'Estació*, *Sallent*. Interferometric phase due to the APS between images separated in time (d) 15 min (e) 1 h, and (f) 4 h approximately.

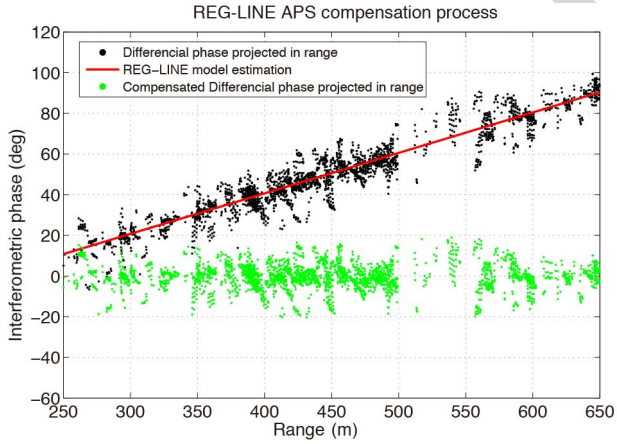

F3:1 Fig. 3. Compensation process of an interferogram with a temporal span of 2 h
F3:2 over those points with a coherence value over 0.95. Black dots represent the
F3:3 projection of the interferometric phase onto the range axis. Red line accounts
F3:4 for the estimated APS using a linear regression. Green dots correspond to the
F3:5 interferometric phase once it has been compensated for.

exhibits a strong linear behavior in the range direction. The red line represents the estimated APS using the linear regression method indicated in [52] and [59]. Finally, the green dots correspond to the compensated interferometric phase. Notice how the final interferometric phase has a mean value close to zero. This value is normal since during this short temporal span the interferometric phase may be considered totally independent of any deformation process. In other words, within the same measurement day no detectable movements are expected. Indeed, the interferometric phase of APS-free interferograms has a mean value close to zero.

Due to the large number of high-coherent scatterers available in urban scenarios, the basis-based method explained in [52], which uses a set short-time compensation functions between consecutive daily temporal-averaged images, is not required. Exploiting polarimetry at this point is not necessary for the same reason as well.

Finally, in order to reduce the effects of urban target short-time instability induced by human activities, the sample selection technique proposed in [61] is employed for the generation of time-averaged SLC images. The detection of the long-term polarimetric behavior providing the highest number of samples for each day of measurements guaranteed a higher quality of the final interferometric phase information.

D. Displacement Results

The displacement map retrieval process is carried out with the zero-baseline adaptation of the CPT algorithm [52]. The choice of the pixel selection method depends on the number of acquisitions at disposal and on the nature of the scatterers to detect, either distributed or point-like scatterers. For this case, since the number of images available is short, only 9, the coherence stability criterion has demonstrated to perform well. A threshold of mean coherence corresponding to 0.7, which is equivalent to a phase standard deviation of about 15°, with a 5×5 multilook window [62], has been established in order to filter out the noisy pixels from the processing. In this type of urban scenarios, a 5×5 multilook window has demonstrated a good performance to detect man-made structures.

At this point, the processing has been benefited by the use of polarimetric optimization techniques [52]. In particular,

the equal scattering mechanism (ESM) polarimetric optimization method [54] has been selected to improve the quality of interferograms. This is translated in roughly a twofold increase in the number of pixels during the pixel selection step.

Finally, the linear velocity map retrieved using the zero-baseline CPT technique is projected over the vertical as indicated in Section II.

The PSI results obtained with the RiskSAR-X sensor are compared with the results provided by the experts of the ICGC [see Fig. 4(a) and (b)], respectively. On the hand, the ground-truth information was obtained by means of a continuous laser topographic levelling system that monitored a set of positions, indicated as dots in Fig. 4(b), during the same period of the GB-SAR campaign. This discrete set of measurements has been employed to obtain the result provided in the same figure through interpolation. On the other hand, due to the high number of high-coherent pixels in the area, GB-SAR results have also been interpolated in order to ease the comparison with the ground-truth available. A high agreement concerning the spatial description of the deformation process may be observed between both techniques. Notice how the position of the area characterized by the maximum deformation bowl perfectly matches. Despite this, it must be pointed out that GB-SAR measurements lead to a slight overestimation of the displacement rate in the center of the deformation focus, 5 cm/year against the 4.5 cm/year given by the *in situ* ground-truth measurements. The difficulty to install the instrument at a higher elevation, to reach shorter incidence angles and maximize the detection in the LOS direction, could explain this slight discrepancy.

Fig. 4(c) shows the time series of a coherent scatter located in the maximum deformation bowl of the area. A strong linearity, as expected from ground-truth measurements and from the spaceborne results available [57], [58], may be observed.

IV. Landslide Monitoring Study Case

Due to the all-weather and day-night capability to accurately detect ground and surface deformations, GB-InSAR has become a useful tool for geo-hazard assessment during the last few years. The accurate monitoring of landslide surfaces represents an important issue in order to achieve a better understanding of landslide mechanisms, and detecting its potential risks to ensure the safety of people living in such areas.

Traditionally, landslide monitoring has been carried out employing different geotechnical devices, including inclinometers, extensometers, piezometers, and GPS differential networks. These in-field measurements present, in general, a benchmark density and a lower extent compared with SAR techniques. In addition, they require the installation of devices directly onto the landslide surface, which can be a problem when the accessibility to the area is complex. The development of remote sensing monitoring tools based on SAR data is becoming an important issue for many authorities in order to ensure the safety of people living in such areas.

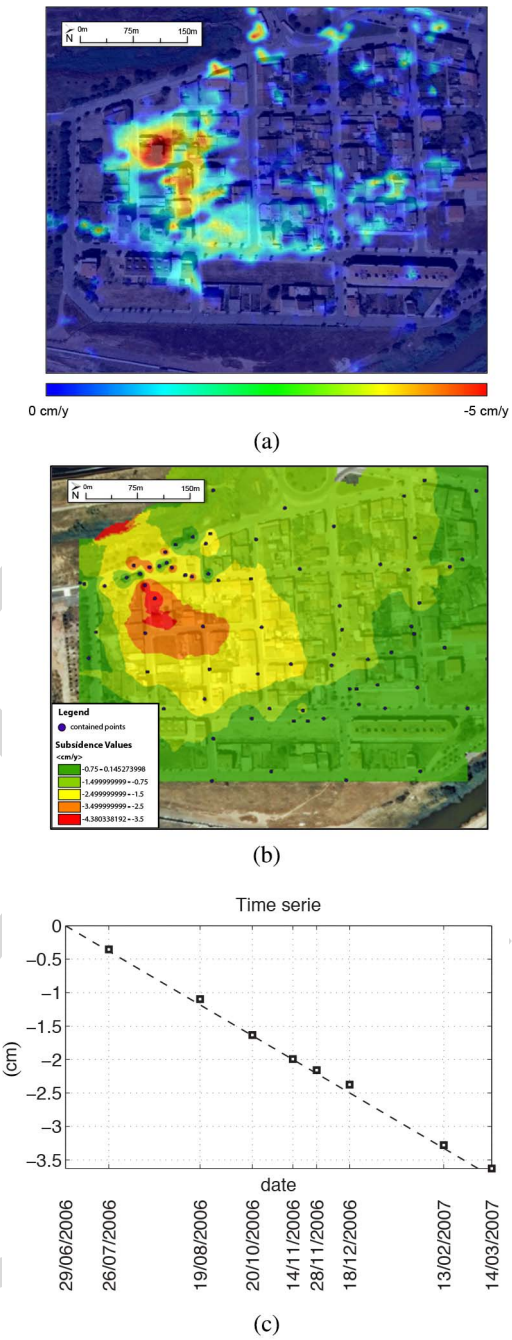

Fig. 4. (a) Vertical linear displacement map retrieved by using the zero-baseline CPT algorithm. (b) Ground-truth map provided by the ICGC employing laser topographic leveling techniques. (c) Displacement time series of a point located in the center of the deformation focus with a linear velocity of 4.7 cm/year. F4:1 F4:2 F4:3 F4:4

A. Test Site and Data Set

The test site selected to demonstrate the applicability of GB-SAR sensors in these applications corresponds to the landslide of *El Forn de Canillo*, located in the Andorran Pyrenees. It has been widely studied since 1980s, and today it is considered as one of the largest landslides of the Pyrenean region [see Fig. 5(a)].

The landslide is composed by a sequence of slides and earthflows with a complex structure, which affects an estimated mass

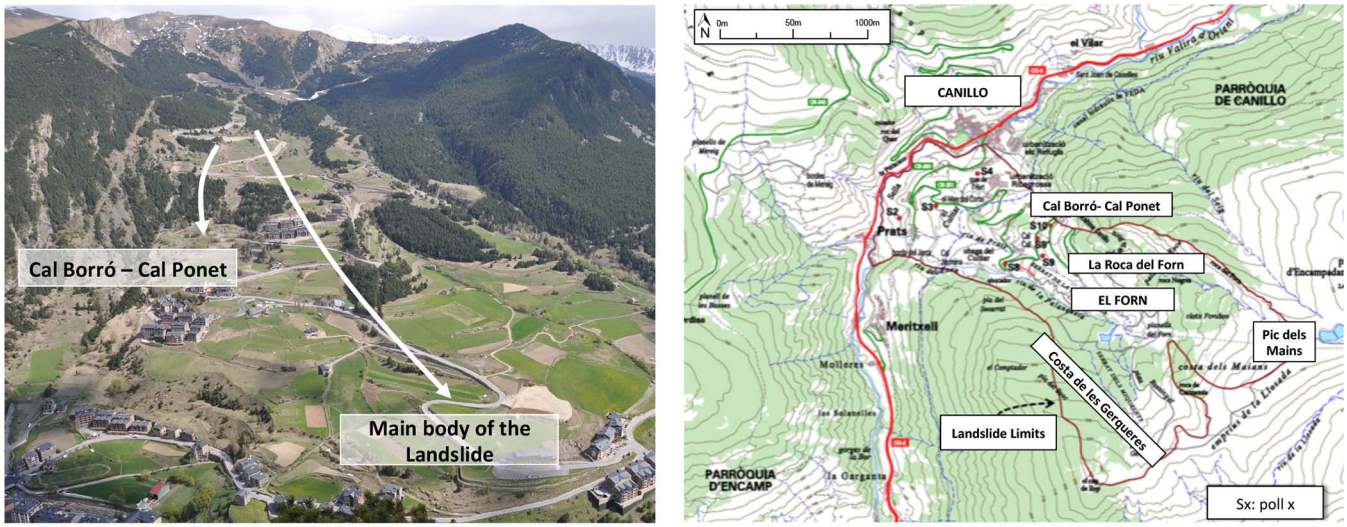

(a) (b)

F5:1 Fig. 5. (a) General overview of the landslide of *El Forn de Canillo*. (b) Landslide limits and location of the devices installed.

at around 300 Mm^3. In this context, three major sliding units were identified in 1994 [63]. The first one corresponds to a slide originated in the area of *Pla del Géspit-Costa de les Gerqueres* [Fig. 5(b)], located in the south-west of the landslide, which reached the foot of the hillside. A second unit was originated under *El Pic de Maians* [see Fig. 5(b)] reaching a height of 1640 m, and that overlaps with the previous sliding unit, closing in the *Valira River* valley. Finally, a new rotational slide with a lower extension originated on the hillside known as *La Roca del Forn* [see Fig. 5(b)] in the north-east side of the hillside has been identified.

The landslide of *El Forn de Canillo* was originated as the result of the hillside destabilization, due to a decompression phenomenon after the removal of the *Valira Glacier*, between 13 000 and 16 000 years before present [63]. The *Valira River* has been progressively eroding the base of the whole mass without reaching the bedrock, and thus originating the landslide.

The geological observations accumulated during the last decades have evidenced the presence of a main slide mass with a residual movement of some millimeters per year, accompanied by a local failure in the area known as *Cal-Ponet Cal-Borró* [see Fig. 5(b)] within the third slide unit described above. This slide is presenting today a major activity coinciding with periods of strong rainfalls and snow melting.

In front of all these evidences, the authorities promoted several actions in the year 2000 for the management of the risk related with the geo-hazard threats associated with landslides, rockfalls, and debris flows in the Andorran Pyrenees. Some specific management plans were carried out for the monitoring of *El Forn de Canillo*.

Between 2007 and 2009, a complex network of geotechnical devices, including inclinometers, rod extensometers, and piezometers, was installed in order to characterize and understand the dynamics of the landslide. A total of 10 boreholes, referred from *S1* to *S10* in Fig. 5(b), reaching a depth between 40 and 60 m, were drilled and equipped with this instrumentation. The measurements provided by these devices have been recently studied with the objective of locating the sliding surfaces and characterizing the displaced material [64].

Unfortunately, some of the boreholes did not reach the needed depth, and consequently the installed devices did not work properly in some points. Despite this, as it has been expected from *in situ* observations, the installed devices evidenced that, in addition to a residual movement of the main lobe of some millimeters per year, the most active part of the landslide corresponds to the secondary landslide of *Cal Borró-Cal Ponet*, which between May and June 2009 registered a velocity up to roughly 2 cm/month [64]. Intense rain events and sudden snow melting was observed during this period. As an example, a famous house built in the mid-19th century, located next to the foot of this secondary landslide near to *S10*, has experienced a significant damage [see Fig. 6(a)]. Several cracks and shear openings along the road pavements close to this area have also appeared over the last years [see Fig. 6(b)].

In 2011, the use of GB-InSAR techniques to identify and characterize the dynamics of the landslide were planned. The reasons were twofold: on the hand, most of the geotechnical devices implemented did not work properly providing unreliable measures and, on the other hand, conventional geotechnical field measurements present lower densities and thus a worse coverage compared with SAR techniques. For this reason, the RSLab, in collaboration with the Department of Geotechnical Engineering and Geosciences of the UPC, carried out a 1-year measurement campaign, from October 2010 to October 2011, with the objective of identifying and characterizing the behavior of the landslide.

Since the landslide of *El Forn de Canillo* is nowadays quite stable with some residual movement of the order of few centimeters per year, a continuous monitoring was considered clearly unfruitful. For this reason, a total of 10 daily data sets were collected with a temporal base line of approximately 1 month, performing thus a discontinuous monitoring, sufficient to avoid phase unwrapping (see Table II).

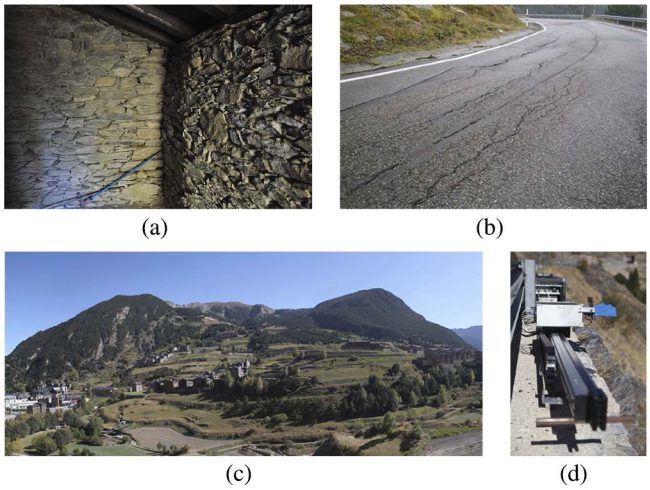

F6:1 Fig. 6. (a) Interior view of the cracked walls of a small farmhouse located in
F6:2 the area of *Cal Borró-Cal Ponet*. The curved shape of the wall indicate the
F6:3 presence of displacements in this area. (b) Cracks and shear openings along a
F6:4 road pavement close to the area of *Cal Borró-Cal Ponet*. (c) Panoramic view of
F6:5 *El Forn de Canillo*, in the Andorran Pyrenees from (d) the RiskSAR point of
F6:6 view.

T2:1 TABLE II
T2:2 TIMETABLE OF EL FORN DE CANILLO MEASUREMENT DAYS

Campaign	Date dd/mm/yyyy	Start Time hh:mm	Stop Time hh:mm	Numb. of Scans
1	21/10/2010	09:57	12:08	15
2	18/11/2010	17:04	19:13	24
3	09/02/2011	17:00	19:48	33
4	07/04/2011	18:17	23:30	60
5	06/05/2011	10:02	11:47	22
6	25/05/2011	16:09	20:08	50
7	09/06/2011	13:20	16:32	51
8	05/07/2011	08:25	12:24	52
9	06/09/2011	11:49	04:05	88
10	05/10/2011	11:57	16:42	66

B. System Setup

The RiskSAR-X sensor was located at the foot of the landslide, 100 m away from the slope, in order to reduce the foreshortening and to maximize the detection of the deformation considering that the landslide moves along the steepest gradient of the terrain slope, as seen in Section II. This emplacement also allows overcoming the geographical accidents of the scenario in order to avoid shadowing in SAR images.

The final area of observation was approximately 500 m in height, 1600 m in range, and 1000 m in width. In addition, as in the urban monitoring case, the system was placed on a base at the height of approximately 30 cm above the ground, to level the rail and avoid the impact of the nearby vegetation in the measurements. As in the previous study case, each scan took roughly 2.5 min to perform a fully polarimetric measure.

A picture of the RiskSAR-X point of view and the sensor's location is detailed in Fig. 6(c) and (d), respectively.

C. Short-Term and Long-Term Processing

Regarding the characteristics of the scenario, *El Forn de Canillo* is mainly covered by vegetation and only contains some man-made structures and few rocky areas suitable to perform a reliable GB-InSAR processing. The reflectivity image of the region covered by the RiskSAR-X sensor is shown in Fig. 7(a). Fig. 7(b) and (c) shows the coherence maps of image pairs with a temporal baseline of 13 min and 6 h, respectively.

Notice how the high-reflectivity areas generally correspond to those pixels with higher coherence values, as expected. These pixels belong to man-made structures, rocky areas, or bare surfaces. Notice also how coherence decreases faster on vegetated areas at X-band, and how only man-made structures or rocky areas remain coherent along time. A considerable loss of coherence in only 6 h can be noticed. Preserving high-coherent pixels along time is a critical issue in these vegetated scenarios, as seen hereinafter.

As in the urban subsidence study case, some important aspects about the STP and LTP [52] processing must remarked prior applying PSI techniques.

Regarding the APS, contrarily to the study case of urban areas seen above, mountainous regions present severe atmospheric phase fluctuations, mainly due to the presence of steep topography. Those regions exhibit strong fluctuations of the atmospheric parameters such as temperature, pressure, and humidity from acquisition to acquisition. Due to this reason, the spatial homogeneity assumption, fulfilled in the previous case, does no longer apply. This fact produces the refractivity index to change in both, the spatial domain, mainly due to the changes in the height, and the temporal one, mainly due to the more extreme atmospheric conditions. The linear-regression model, seen in the urban study case needs to be updated with a second-order term related with the product of range distance and height [52], [60].

In order to illustrate that problem, Fig. 7(d)–(f) is presented. This figure shows the temporal evolution of the interferometric phase after only 1 h. Severe atmospheric phase fluctuations, highly correlated with the steep topography of the scenario, appear in just 1 h leading to over one-cycle phase variations [see Fig. 7(f)].

Fig. 8 shows how the linear-regression model used in the urban study case is not sufficient to compensate for the APS in these scenarios. The compensation process for this example is carried out over an interferogram with a temporal span of only 1 h. The black dots represent the projection of the interferometric phase onto the range axis in the pixels of the image with higher coherence values ($\gamma > 0.95$). Notice how the interferometric phase does no longer exhibit a linear behavior in the range direction. The red line represents the estimated APS using a linear regression, which considerably departs from the interferometric phase, especially at the near and far range. The blue points refer to the new model, indicated in [52] and [60], which accounts for the height of the scenario. Notice how it perfectly fits the interferometric phase trend. Finally, the green dots correspond to the interferometric phase after the compensation process showing the goodness of the proposed technique.

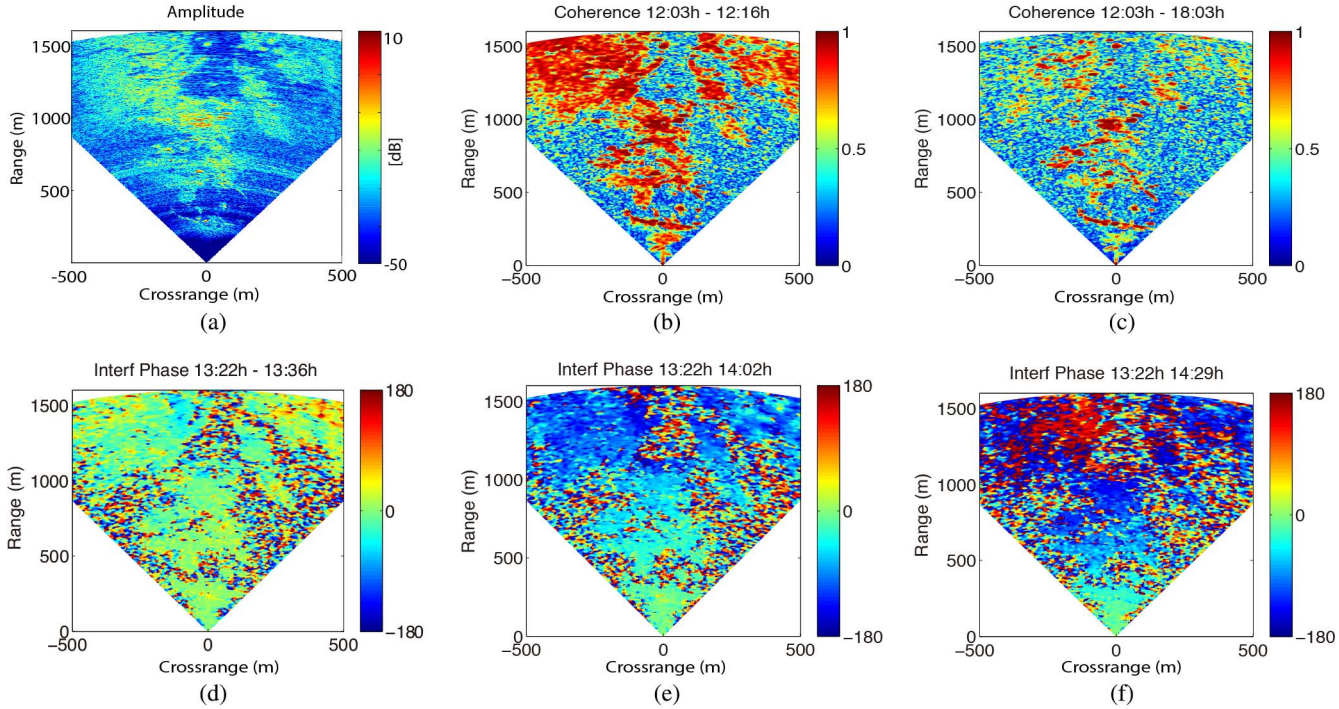

F7:1 Fig. 7. (a) Reflectivity image in dB and coherence maps between acquisitions with a temporal baseline of (b) 13 min and (c) 6 h corresponding to the area of
F7:2 *El Forn de Canillo*, Andorra. Interferometric phase due to APS between images separated in time (d) 15 min (e) 30 min, and (f) 1 h approximately.

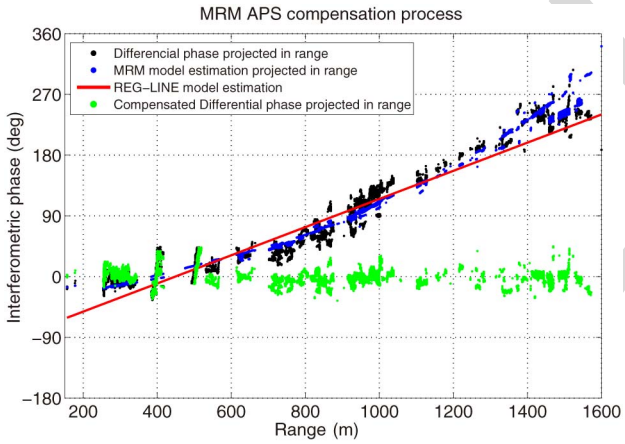

F8:1 Fig. 8. Compensation process of an interferogram with a temporal span of 1 h
F8:2 over those points with a coherence value over 0.95. Black dots represent the
F8:3 projection of the interferometric phase onto the range axis. Red line accounts
F8:4 for the estimated APS using a linear regression. Blue dots refer to the estimated
F8:5 APS using a multiple regression model that takes into account the height of the
F8:6 scenario. Green dots correspond to the interferometric phase once it has been
F8:7 compensated for.

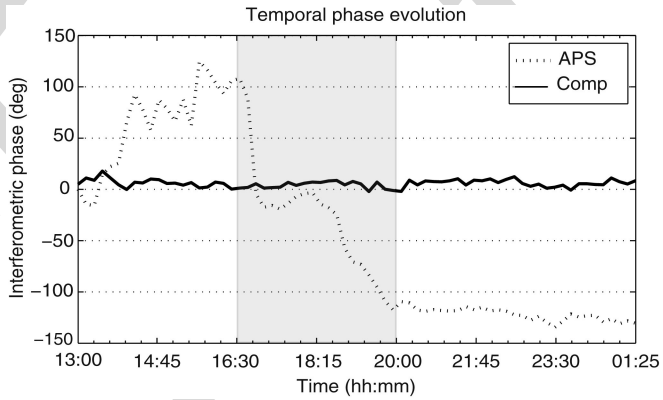

F9:1 Fig. 9. Phase evolution of a coherent scatterer ($\gamma = 0.97$ using a 9×9 mul-
F9:2 tilook) along 70 measures collected during 12 h, from 1:00 P.M. to 1:25 A.M.,
F9:3 every 10 min. The dotted line refers to the phase evolution before applying the
F9:4 APS compensation step. The solid line accounts for the phase evolution once
F9:5 the APS is compensated for. The shaded area accounts for the sunset period,
F9:6 coinciding with the more severe APS fluctuations.

Fig. 9 illustrates the good performance of the APS compensation technique along time. This figure presents the phase evolution of a coherent scatterer ($\gamma = 0.97$ using a 9×9 multilook) along a total of 70 measures collected during 12 h, from 1:00 P.M. to 1:25 A.M., every 10 min. The dotted line refers to the phase evolution before applying the APS compensation step meanwhile, the solid one accounts for the phase evolution once the APS is compensated. Since all the measures belong to the same measurement day, it is expected an absence of movement. After performing the APS compensation step, the interferometric phase (solid line) presents a zero-mean value with a low standard deviation value, $\sigma = 3.6°$, which corresponds to 0.16 mm. This experiment demonstrates the good performance of the technique over these kind of scenarios. Fig. 9 also illustrates how the atmosphere fluctuations are more severe during the day, and especially at sunset (shaded area). This fact confirms that the best GB-SAR performances may be achieved measuring at night, especially in these type of mountainous environments.

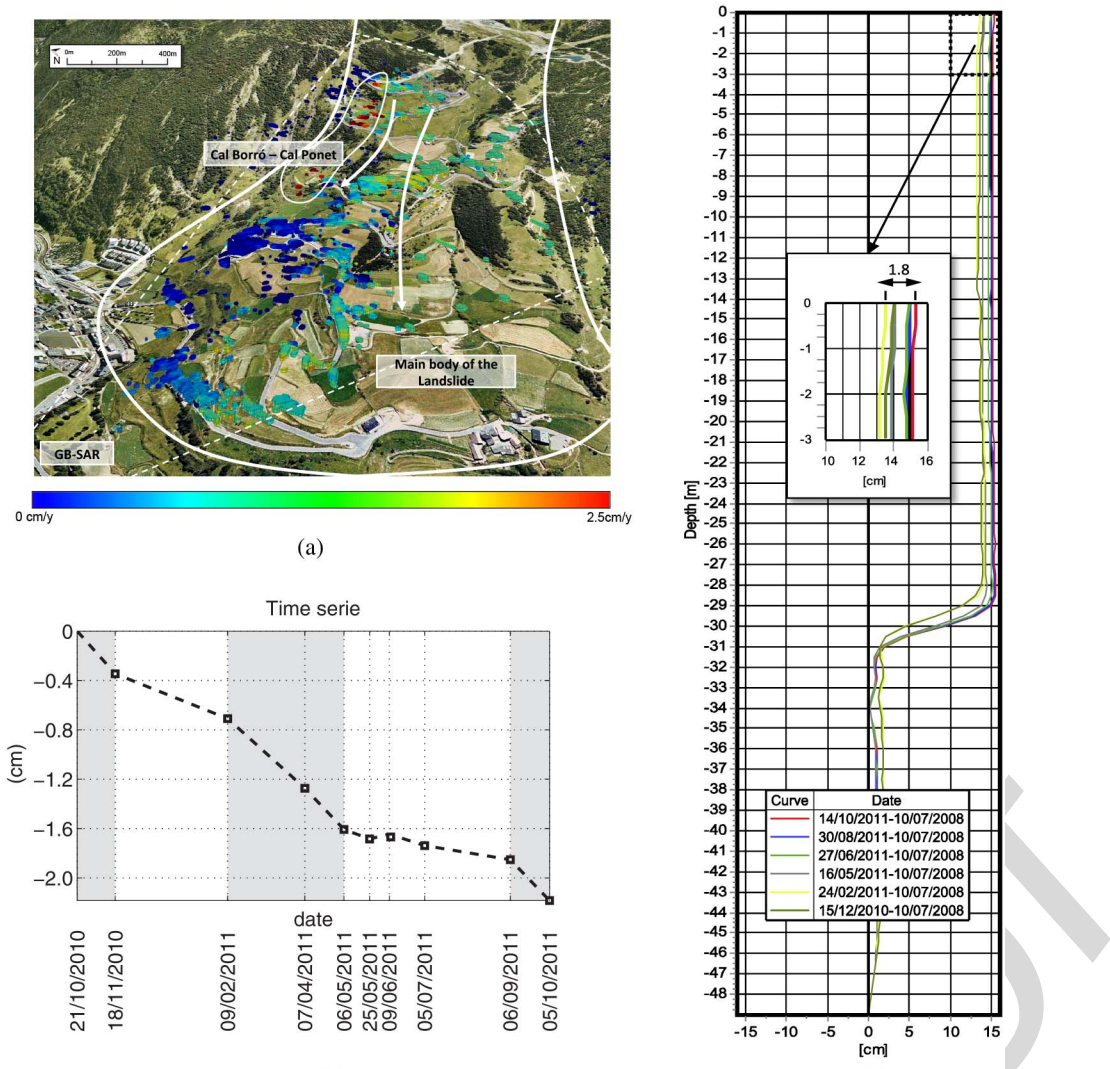

F10:1 Fig. 10. (a) Geocoded down-slope linear ground-displacement of *El Forn de Canillo* obtained with the RiskSAR-X sensor covering the period from October 2010
F10:2 to October 2011. (b) Displacement time series of a point located in the area of *Cal Borró-Cal Ponet* with a linear velocity of $\sim 2.3\,\mathrm{cm/year}$. The shaded areas
F10:3 indicate the periods when the landslide experienced major accelerations. (c) Inclinometric results provided by the firm *Euroconsult* in the borehole *S10*, located in
F10:4 the area of *Cal Borró-Cal Ponet*.

At this stage, maximizing the chances of detecting the major number of coherent scatterers available within the area of study is mandatory.

On the one hand, the LTP has been benefited from the use of the compensating function method described in [52]. This method seeks to perform the APS estimation and compensation process using the shortest temporal baselines available in the data set. A basis of short-term compensation functions between consecutive daily temporal-averaged images, characterized by a minimum loss of coherence are first generated. Then, these are employed to compensate for long-term span interferograms.

On the other hand, the LTP may also be benefited from the use of PolSAR data [52], [60]. A simple strategy, which notably increases the number of coherent scatters selected, consists of selecting for each interferogram which needs to be compensated for, the polarimetric channel providing the highest coherence value. This strategy leads to a twofold increase in the number of high-quality pixels during APS compensation step.

D. Displacement Results

The displacement map retrieval is carried out with the zero-baseline adaptation of the CPT technique [52].

Since the number of images available is short, 10 images, the coherence stability criterion is proposed to carry out the pixel selection. This approach performs well even when a reduced number of images are available. Moreover, this pixel selection criterion has demonstrated to be more suited in natural environments with predominance of distributed scatters.

At this point, since the number of high-quality pixels is smaller for this environment, the zero-baseline CPT algorithm is benefited by the use of a multilayer processing [65].

Two thresholds of mean coherence corresponding to 0.7 and 0.6 are fixed. These correspond to phase standard deviations of about 15° and 20°, respectively, using a 5×5 multilook window [62]. This multilook window maximizes the detection of stable coherent scatters coming from both man-made structures and natural targets, such as rocky areas or bare surfaces.

Furthermore, the ESM polarimetric optimization method [54] has also been employed in order to improve the phase quality of interferograms, and thus achieve a dense network of coherent scatterers to carry out a reliable PSI processing.

Fig. 10(a) shows the final down-slope linear ground-displacement map geocoded over a Google Earth image, using the zero-baseline CPT algorithm. The result shows a high agreement with the conclusions extracted from the field monitoring campaigns made between 2007 and 2009, presented in [64]. Concretely, the displacement map obtained reveals that the main body of the landslide experienced a residual movement of approximately 1 cm/month during the period of observation. In the top-left, part of the hillside a local landslide presenting a higher activity ($\sim 2-2.5$ cm/year) may be appreciated. It corresponds to the so-called secondary landslide of *Cal Borró-Cal Ponet*, described previously. Fig. 10(b) shows the temporal evolution of a high-coherence point belonging to the maximum displacement rate area. Unlike the urban subsidence case studied previously, which was characterized by a strong linear component, the temporal evolution of the displacement has now a strong nonlinear component. It presents several accelerations and stabilizations during the period of measures. The shaded areas in the figure indicate the periods when the landslide experienced major accelerations. Analyzing the figure in detail, it can be observed that the major displacements are produced in the fall (from October to November 2010) and spring (from February to June 2011), coinciding with the major rainfall and snow melting events. In the last period of the graph (September 2011), coinciding again with autumn's arrival, the landslide seems to accelerate again.

Finally, Fig. 10(c) shows the inclinometric results provided by the firm Euroconsult in the borehole *S10*, located in the maximum deformation rate area of *Cal Borr-Cal Ponet*. The figure illustrates a horizontal profile of the deformed shape of the inclinometer casing along the borehole depth in the down-slope direction for different dates. The curves correspond to the period corresponding from December 2010 to October 2011, and all are referred to July 2008. The S-shaped plot reflects that the main shear band is located about 30 m under the surface of the landslide. In order to ease the comparison of the inclinometric results with the ones obtained with the GB-SAR sensor, the upper part of the plot has been amplified. Since the inclinometric results are given in an horizontal plane, these must be divided by the cosine of the slope angle at *S10* ($\sim 20^\circ$) in order to obtain the total down-slope displacement. Notice how during the period from December 2012 to October 2013, the movement along the maximum-slope according to the inclinometer is $\sim 1.8\,\mathrm{cm}/\cos(20^\circ) = 1.91\,\mathrm{cm}$. This corresponds to roughly ~ 2.3 cm/year. Results provided by the GB-SAR are ~ 2.5 cm/year in this area showing a high agreement with the ground truth provided, and demonstrating again the good performance of GB-SAR sensors for the study of ground displacement monitoring applications.

V. Conclusion

Urban subsidence and landslide instabilities involve a wide range of issues that are of concern to governments at all levels. Increasingly, authorities are promoting actions when they threaten public or private properties and, especially, human life, in order to mitigate the socioeconomic losses derived from these problems.

This paper seeks to demonstrate the usefulness of GB-InSAR and PSI techniques, for the monitoring of different kinds of ground displacement phenomena. With this purpose, two different scenarios have been monitored using the RiskSAR sensor and the GB-InSAR processing chain developed by the RSLab [52]. One is an urban area affected by mining induced subsidence and the other a mountainous landslide. For both cases, the obtained deformation maps have been validated with in-field ground-truth data. In addition, the key logistics' particularities and processing approach have been deeply analyzed depending on the nature of the area and the ground displacement process to be monitored. Concretely, the APS estimation and compensation step, which represents one of the most critical aspects in GB-InSAR, has been deeply discussed for each scenario.

The reliability of GB-SAR products has been demonstrated, representing an effective alternative for the design and implementation of prevention strategies, showing a high feasibility to hazard assessment and risk management.

Compared with PSI spaceborne solutions, GB-SAR sensors present several advantages due to the zero-baseline configuration of the instrument, which is firmly anchored on the same position for all acquisitions. The revisiting time is no longer a constraint due to the employment of a terrestrial platform. In addition, they offer the possibility to fit the illumination angle in order to maximize the detection of real ground displacement in the LOS direction. Anyway, this is strongly dependent on the characteristics of the site and in some cases it could not be possible. For instance, for urban subsidence monitoring not always there will be a nearby cliff. Finally, since APS may be perfectly estimated and compensated for, lower numbers of images are required in order to achieve reliable nonlinear estimations of the ground displacement processes. Compared with traditional in-field monitoring devices and techniques, including total stations, differential GPS, geological mapping, geophysical prospection, topographic leveling, extensometers, inclinometers, and piezometers, GB-SAR solutions have demonstrated to provide higher densities and to be very efficient in order to cover larger areas for long periods at lower cost.

Some future work lines may include the extension of the APS model-based techniques proposed in this paper for the monitoring of large-scale scenarios characterized by several kilometers in range. Moreover, the ability to solve unwrapping errors when facing more complex terrains and larger illuminated areas should be deeply analyzed.

ACKNOWLEDGMENT

The authors would like to thank Prof. J. Corominas and J. A. Gili from the Department of Geotechnical Engineering and Geosciences, Universitat Politècnica de Catalunya (UPC), their helpful discussions and support in the interpretation of the final displacement results over the test site of *El Forn de Canillo*. They also wish to thank the Institut Cartogràfic i Geològic de Catalunya (ICGC) for the ground-truth map provided in the test-site of *Sallent*, and finally, the firm Euroconsult for the inclinometric results for the test-site of *El Forn de Canillo*.

REFERENCES

[1] D. Massonnet and K. L. Feigl, "Radar interferometry and its application to changes in the Earth's surface," *Rev. Geophys.*, vol. 36, no. 4, p. 441, 1998.

[2] R. Bürgmann, P. A. Rosen, and E. J. Fielding, "Synthetic aperture radar interferometry to measure Earth's surface topography and its deformation," *Annu. Rev. Earth Planetary Sci.*, vol. 28, no. 1, pp. 169–209, May 2000.

[3] A. K. Gabriel, R. M. Goldstein, and H. A. Zebker, "Mapping small elevation changes over large areas: Differential radar interferometry," *J. Geophys. Res.*, vol. 94, no. B7, p. 9183, 1989.

[4] A. Ferretti, C. Prati, and F. Rocca, "Nonlinear subsidence rate estimation using permanent scatterers in differential SAR interferometry," *IEEE Trans. Geosci. Remote Sens.*, vol. 38, no. 5, pp. 2202–2212, Sep. 2000.

[5] A. Ferretti, C. Prati, and F. Rocca, "Permanent scatterers in SAR interferometry," *IEEE Trans. Geosci. Remote Sens.*, vol. 39, no. 1, pp. 8–20, Jan. 2001.

[6] O. Mora, J. J. Mallorqui, and J. Duro, "Generation of deformation maps at low resolution using differential interferometric SAR data," in *Proc. IEEE Int. Geosci. Remote Sens. Symp.*, 2002, vol. 5, pp. 2696–2698.

[7] P. Berardino, G. Fornaro, R. Lanari, and E. Sansosti, "A new algorithm for surface deformation monitoring based on small baseline differential SAR interferograms," *IEEE Trans. Geosci. Remote Sens.*, vol. 40, no. 11, pp. 2375–2383, Nov. 2002.

[8] O. Mora, J. Mallorqui, and A. Broquetas, "Linear and nonlinear terrain deformation maps from a reduced set of interferometric SAR images," *IEEE Trans. Geosci. Remote Sens.*, vol. 41, no. 10, pp. 2243–2253, Oct. 2003.

[9] C. Werner, U. Wegmuller, T. Strozzi, and A. Wiesmann, "Interferometric point target analysis for deformation mapping," in *Proc. IEEE Int. Geosci. Remote Sens. Symp. (IGARSS'03)*, 2003, vol. 7, pp. 4362–4364.

[10] A. Arnaud *et al.*, "ASAR ERS interferometric phase continuity," in *Proc. IEEE Int. Geosci. Remote Sens. Symp.*, 2003, vol. 2, pp. 1133–1135.

[11] A. Hooper, "A new method for measuring deformation on volcanoes and other natural terrains using InSAR persistent scatterers," *Geophys. Res. Lett.*, vol. 31, no. 23, p. L23611, 2004.

[12] R. Lanari *et al.*, "A small-baseline approach for investigating deformations on full-resolution differential SAR interferograms," *IEEE Trans. Geosci. Remote Sens.*, vol. 42, no. 7, pp. 1377–1386, Jul. 2004.

[13] A. Hooper, "A multi-temporal InSAR method incorporating both persistent scatterer and small baseline approaches," *Geophys. Res. Lett.*, vol. 35, no. 16, p. L16302, Aug. 2008.

[14] G. Fornaro, D. Reale, and F. Serafino, "Four-dimensional SAR imaging for height estimation and monitoring of single and double scatterers," *IEEE Trans. Geosci. Remote Sens.*, vol. 47, no. 1, pp. 224–237, Jan. 2009.

[15] A. Ferretti *et al.*, "A new algorithm for processing interferometric datastacks: SqueeSAR," *IEEE Trans. Geosci. Remote Sens.*, vol. 49, no. 9, pp. 3460–3470, Sep. 2011.

[16] D. Tarchi *et al.*, "SAR interferometry for structural changes detection: A demonstration test on a DAM," in *Proc. IEEE Int. Geosci. Remote Sens. Symp. (IGARSS'99)*, 1999, vol. 3, pp. 1522–1524.

[17] H. Rudolf, D. Leva, D. Tarchi, and A. Sieber, "A mobile and versatile SAR system," in *Proc. IEEE Int. Geosci. Remote Sens. Symp. (IGARSS'99)*, 1999, vol. 1, pp. 592–594.

[18] D. Leva, G. Nico, D. Tarchi, J. Fortuny-Guasch, and A. Sieber, "Temporal analysis of a landslide by means of a ground-based SAR interferometer," *IEEE Trans. Geosci. Remote Sens.*, vol. 41, no. 4, pp. 745–752, Apr. 2003.

[19] S. Brown, S. Quegan, K. Morrison, J. Bennett, and G. Cookmartin, "High-resolution measurements of scattering in wheat canopies-implications for crop parameter retrieval," *IEEE Trans. Geosci. Remote Sens.*, vol. 41, no. 7, pp. 1602–1610, Jul. 2003.

[20] G. Nico, D. Leva, G. Antonello, and D. Tarchi, "Ground-based SAR interferometry for terrain mapping: Theory and sensitivity analysis," *IEEE Trans. Geosci. Remote Sens.*, vol. 42, no. 6, pp. 1344–1350, Jun. 2004.

[21] G. Luzi *et al.*, "Ground-based radar interferometry for landslides monitoring: atmospheric and instrumental decorrelation sources on experimental data," *IEEE Trans. Geosci. Remote Sens.*, vol. 42, no. 11, pp. 2454–2466, Nov. 2004.

[22] A. Aguasca, A. Broquetas, J. J. Mallorqui, and X. Fabregas, "A solid state L to X-band flexible ground-based SAR system for continuous monitoring applications," in *Proc. IEEE Int. Geosci. Remote Sens. Symp. (IGARSS'04)*, 2004, vol. 2, pp. 757–760.

[23] L. Pipia, A. Aguasca, X. Fabregas, and J. Mallorqui, "A polarimetric ground-based SAR system: First results at X-band," in *Proc. URSI Commiss. F Symp. Microw. Remote Sens. Earth Oceans Ice Atmos.*, Ispra, Italy, Jul. 2005.

[24] L. Noferini *et al.*, "Permanent scatterers analysis for atmospheric correction in ground-based SAR interferometry," *IEEE Trans. Geosci. Remote Sens.*, vol. 43, no. 7, pp. 1459–1471, Jul. 2005.

[25] M. Pieraccini, G. Luzi, and C. Atzeni, "Ground-based interferometric SAR for terrain elevation mapping," *Electron. Lett.*, vol. 36, no. 16, pp. 1416–1417, 2000.

[26] Z.-S. Zhou, W.-M. Boerner, and M. Sato, "Development of a ground-based polarimetric broadband SAR system for noninvasive ground-truth validation in vegetation monitoring," *IEEE Trans. Geosci. Remote Sens.*, vol. 42, no. 9, pp. 1803–1810, Sep. 2004.

[27] G. Bernardini, P. Ricci, and F. Coppi, "A ground based microwave interferometer with imaging capabilities for remote measurements of displacements," *Geotelematics Fair*, 2007.

[28] C. Werner, T. Strozzi, A. Wiesmann, and U. Wegmüller, "GAMMA's portable radar interferometer," *Proc. 13th FIG Symp. Deform. Meas. Anal.*, 2008, pp. 1–10.

[29] L. Pipia, "Polarimetric differential SAR interferometry with ground-based sensors," Ph.D. dissertation, Universitat Politècnica de Catalunya, Barcelona, Spain, 2009.

[30] K. Lukin and A. Mogyla, "Monitoring of St. Sophia Cathedral interior using Ka-band ground based noise waveform SAR," in *Proc. 6th Radar Conf., (EURAD'09)*, Rome, Italy, 2009, pp. 215–217.

[31] C. Del Ventisette *et al.*, "Using ground-based radar interferometry during emergency: The case of the A3 motorway (Calabria Region, Italy) threatened by a landslide," *Natural Hazards Earth Syst. Sci.*, vol. 11, no. 9, pp. 2483–2495, Sep. 2011.

[32] S. Rodelsperger, A. Coccia, D. Vicente, and A. Meta, "Introduction to the new metasensing ground-based SAR: Technical description and data analysis," in *Proc. IEEE Int. Geosci. Remote Sens. Symp.*, Jul. 2012, pp. 4790–4792.

[33] H. Lee, S. Member, J.-H. Lee, S. Member, and K.-E. Kim, "Development of a truck-mounted arc-scanning synthetic aperture radar," *IEEE Trans. Geosci. Remote Sens.*, vol. 52, no. 5, pp. 2773–2779, May 2014.

[34] N. Harries, D. Noon, H. Pritchett, and D. Bates, "Slope stability radar for managing rock fall risks in open cut mines," in *Proc. 3rd CANUS Rock Mech. Symp.*, Toronto, ON, Canada, May 2009, vol. 2009, pp. 1–8.

[35] D. Mecatti *et al.*, "Monitoring open-pit quarries by interferometric radar for safety purposes," in *Proc. 7th Eur. Radar Conf.*, Paris, France, Oct. 2010, pp. 37–40.

[36] P. Farina *et al.*, "IBIS-M: An innovative radar for monitoring slopes in open-pit mines," in *Proc. Int. Symp. Rock Slope Stabil. Open Pit Mining Civil Eng.*, Vancouver, BC, Canada, 2011.

[37] P. Farina and N. Coli, "Efficient real time stability monitoring of mine walls : The Çöllolar mine case study," in *Proc. Int. Mining Congr. Exhib. Turkey*, Antalya, Turkey, 2013, pp. 111–117.

[38] D. Tarchi *et al.*, "On the use of ground-based SAR interferometry for slope failure early warning: The Cortenova rock slide (Italy)," in *Landslides*, 2005, pp. 337–342.

[39] D. Tarchi, "Monitoring landslide displacements by using ground-based synthetic aperture radar interferometry: Application to the Ruinon landslide in the Italian Alps," *J. Geophys. Res.*, vol. 108, no. B8, p. 2387, 2003.

[40] N. Casagli, F. Catani, C. Del Ventisette, and G. Luzi, "Monitoring, prediction, and early warning using ground-based radar interferometry," *Landslides*, vol. 7, no. 3, pp. 291–301, May 2010.

[41] M. Pieraccini *et al.*, "Remote sensing of building structural displacements using a microwave interferometer with imaging capability," *NDT & E Int.*, vol. 37, no. 7, pp. 545–550, 2004.

[42] L. Pipia *et al.*, "Polarimetric differential SAR interferometry: First results with ground-based measurements," *IEEE Geosci. Remote Sens. Lett.*, vol. 6, no. 1, pp. 167–171, Jan. 2009.

[43] M. Crosetto, O. Monserrat, G. Luzi, M. Cuevas-González, and N. Devanthéry, "Discontinuous GBSAR deformation monitoring," *ISPRS J. Photogramm. Remote Sens.*, vol. 93, pp. 136–141, Jul. 2014.

[44] D. Tarchi, E. Ohlmer, and A. Sieber, "Monitoring of structural changes by radar interferometry," *Res. Nondestruct. Eval.*, vol. 9, no. 4, pp. 213–225, Jan. 1997.

[45] O. Montserrat, "Deformation measurement and monitoring with Ground-Based SAR," Ph.D. dissertation, Institute of Geomatics, Barcelona, Spain, 2012.

[46] L. Noferini, D. Mecatti, G. Macaluso, M. Pieraccini, and C. Atzeni, "Monitoring of Belvedere Glacier using a wide angle GB-SAR interferometer," *J. Appl. Geophys.*, vol. 68, no. 2, pp. 289–293, Jun. 2009.

[47] D. Tarchi, "Monitoring landslide displacements by using ground-based synthetic aperture radar interferometry: Application to the Ruinon landslide in the Italian Alps," *J. Geophys. Res.*, vol. 108, no. B8, p. 2387, 2003.

[48] G. Herrera *et al.*, "A landslide forecasting model using ground based SAR data: The Portalet case study," *Eng. Geol.*, vol. 105, no. 3–4, pp. 220–230, May 2009.

[49] G. Barla, F. Antolini, M. Barla, E. Mensi, and G. Piovano, "Monitoring of the Beauregard landslide (Aosta Valley, Italy) using advanced and conventional techniques," *Eng. Geol.*, vol. 116, no. 3–4, pp. 218–235, Nov. 2010.

[50] K. Takahashi, M. Matsumoto, and M. Sato, "Continuous observation of natural-disaster-affected areas using ground-based SAR interferometry," *IEEE J. Sel. Topics Appl. Earth Observ. Remote Sens.*, vol. 6, no. 3, pp. 1286–1294, Jun. 2013.

[51] O. Monserrat, M. Crosetto, and G. Luzi, "A review of ground-based SAR interferometry for deformation measurement," *ISPRS J. Photogramm. Remote Sens.*, vol. 93, pp. 40–48, Jul. 2014.

[52] R. Iglesias *et al.*, "Ground-based polarimetric SAR interferometry for the monitoring of Terrain displacement phenomena. Part I: Theoretical description," to be published.

[53] V. D. Navarro-Sanchez, J. M. Lopez-Sanchez, and L. Ferro-Famil, "Polarimetric approaches for persistent scatterers interferometry," *IEEE Trans. Geosci. Remote Sens.*, vol. 52, no. 3, pp. 1667–1676, Mar. 2014.

[54] R. Iglesias *et al.*, "Phase quality optimization in polarimetric differential SAR interferometry," *IEEE Trans. Geosci. Remote Sens.*, vol. 52, no. 5, pp. 2875–2888, May 2014.

[55] R. Iglesias *et al.*, "Polarimetric optimization of temporal sublook coherence for DInSAR applications," *IEEE Geosci. Remote Sens. Lett.*, vol. 12, no. 1, pp. 87–91, Jan. 2015.

[56] R. Hanssen, *Radar Interferometry: Data Interpretation and Error Analysis*. Norwell, MA, USA: Kluwer, 2001.

[57] J. Marturià, O. Mora, D. Xifre, P. Martínez, and A. Roca, "DInSAR techniques versus high topographic leveling surveys: The subsidence phenomena in Sallent," in *Proc. ECONGEO'06*, Barcelona, Spain, 2006.

[58] O. Mora, R. Arbiol, and V. Pala, "ICC's project for DInSAR terrain subsidence monitoring of the Catalonian territory," in *Proc. IEEE Int. Geosci. Remote Sens. Symp.*, 2007, pp. 4953–4956.

[59] L. Pipia, X. Fabregas, A. Aguasca, and C. Lopez-Martinez, "Atmospheric artifact compensation in ground-based DInSAR applications," *IEEE Geosci. Remote Sens. Lett.*, vol. 5, no. 1, pp. 88–92, Jan. 2008.

[60] R. Iglesias, "Atmospheric phase screen compensation in ground-based SAR with a multiple-regression model over mountainous regions," *IEEE Trans. Geosci. Remote Sens.*, vol. 52, no. 5, pp. 2436–2449, May 2014.

[61] L. Pipia, X. Fabregas, A. Aguasca, and C. Lopez-Martinez, "Polarimetric temporal analysis of urban environments with a ground-based SAR," *IEEE Trans. Geosci. Remote Sens.*, vol. 51, no. 4, pp. 2343–2360, Apr. 2013.

[62] R. Touzi, A. Lopes, J. Bruniquel, and P. Vachon, "Coherence estimation for SAR imagery," *IEEE Trans. Geosci. Remote Sens.*, vol. 37, no. 1, pp. 135–149, Jan. 1999.

[63] N. Santacana, "Estudi dels grans esllavissaments d'Andorra: Els casos del Forn i del vessant d'Encampadana." Ph.D. dissertation, Universitat Politècnica de Catalunya (UPC), Barcelona, Spain, 1994.

[64] I. Torrebadella *et al.*, "El Deslizamiento del Forn de Canillo en Andorra. Un Ejemplo de Gestión del Riesgo Geológico en Zonas Habitadas en Grandes Deslizamientos," in *Proc. 7th Simposio Nacional sobre Taludes y Laderas Inestables*, Barcelona, Spain, 2009, pp. 403–414.

[65] P. Blanco-Sánchez, J. J. Mallorquí, S. Duque, and D. Monells, "The Coherent Pixels Technique (CPT): An advanced DInSAR technique for nonlinear deformation monitoring," *Pure Appl. Geophys.*, vol. 165, no. 6, pp. 1167–1193, Aug. 2008.

Rubén Iglesias (S'12) was born in Barcelona, Spain, in 1982. He received the M.Sc. degree in telecommunication engineering from the Universitat Politècnica de Catalunya (UPC), Barcelona, Spain, in 2008. He is currently pursuing the Ph.D. degree from UPC, focused on the development of advanced differential synthetic aperture radar interferometry (DInSAR) and polarimetric DInSAR (PolDInSAR) techniques for the detection, monitoring, and characterization of slow-moving landslides with both orbital and ground-based SAR (GB-SAR) data.

From June 2009 to June 2010, he was with the Active Remote Sensing Unit, Institute of Geomatics, Barcelona, Spain, working in several projects related with the application of DInSAR to terrain-deformation monitoring with orbital and GB-SAR data. From June 2010 to March 2014, he was with the Signal Theory and Communications Department (TSC), UPC, working as a Research Assistant in the framework of DInSAR and GB-SAR DInSAR applications. In April 2014, he joined Altamira Information, an experienced Earth Observation Company in Barcelona dedicated to provide ground displacement measurements solutions by using DInSAR techniques.

Albert Aguasca (S'90–M'94) was born in Barcelona, Spain, in 1964. He received the M.Sc. and Ph.D. degrees in telecommunication engineering from the Universitat Politècnica de Catalunya (UPC), Barcelona, Spain, in 1989 and 1993, respectively.

Since 1995, he has been an Associate Professor with the School of Telecommunications Engineering, UPC. His teaching activities involve RF and microwave circuits for communications and radio navigation systems. He has published more than 40 papers on microwave synthetic aperture radar, radiometer systems, and microwave circuits. His research interests include the design and development of synthetic aperture radar and microwave radiometer systems for unmanned aerial vehicle (UAV) platforms.

Xavier Fabregas (S'89–M'93) received the B.S. degree in physics from Barcelona University, Barcelona, Spain, in 1988, and the Ph.D. degree in applied sciences from the Universitat Politècnica de Catalunya (UPC), Barcelona, Spain, in 1995.

In 1990, he joined the Photonic and Electromagnetic Engineering Group, Signal Theory and Communications Department, UPC. Since 1996, he has been an Associate Professor with the UPC. In 2001, he spent an eight-month sabbatical with the Microwaves and Radar Institute (HR), German Aerospace Agency (DLR), Oberpfaffenhofen, Germany. He has published 26 international journal papers and more than 106 conference proceedings and has received a patent. He is a Reviewer in several international journals. His research interests include polarimetric-retrieval algorithms, polarimetric calibration and speckle models, GB SAR sensors and their applications, and time series for multidimensional SAR data applications for urban and terrain deformation monitoring.

Jordi J. Mallorqui (S'93–M'96–SM'13) was born in Tarragona, Spain, in 1966. He received the Ingeniero and Doctor Ingeniero degrees in telecommunications engineering from the Universitat Politècnica de Catalunya (UPC), Barcelona, Spain, in 1990 and 1995, respectively.

Since 1993, he has been teaching with the School of Telecommunications Engineering of Barcelona, UPC, first as an Assistant Professor, later in 1997 as an Associate Professor, and since 2011 as a Full Professor. His teaching activity involves microwaves, radionavigation systems, and remote sensing. He spent a sabbatical year with the Jet Propulsion Laboratory, Pasadena, CA, USA, in 1999, working on interferometric airborne synthetic aperture radar (SAR) calibration algorithms. He is currently working on the application of SAR interferometry to terrain-deformation monitoring with orbital, airborne, and ground data; vessel detection and classification from SAR images; and 3-D electromagnetic (EM) simulation of SAR systems. He has published more than 100 papers on microwave tomography, EM numerical simulation, and SAR processing, interferometry, and differential interferometry in refereed journals and international symposia.

Dani Monells (S'11) was born in Sant Joan de les Abadesses, Spain, in 1981. He received the B.Sc. degree in telecommunication engineering from the Universitat Politècnica de Catalunya (UPC), Barcelona, Spain, in 2008. He is currently pursuing the Ph.D. degree focused on differential synthetic aperture radar interferometry (DInSAR) in orbital platforms, focusing on the exploitation of polarimetric SAR acquisitions (PolSAR), at the Signal Theory and Communications Department (TSC), UPC.

Since 2007, he has been working in several projects for the monitoring of terrain displacements and developing the TSC interferometric chain and processor, in order to give support to the new generation SAR satellites.

Carlos López-Martínez (S'97–M'04–SM'11) received the M.Sc. degree in electrical engineering and the Ph.D. degree from the Universitat Politècnica de Catalunya, Barcelona, Spain, in 1999 and 2003, respectively.

From October 2000 to March 2002, he was with the Frequency and Radar Systems Department (HR), German Aerospace Center (DLR), Oberpfaffenhofen, Germany. From June 2003 to December 2005, he has been with the Image and Remote Sensing Group, SAR Polarimetry Holography Interferometry Radargrammetry (SAPHIR) Team, Institute of Electronics and Telecommunications of Rennes (IETR), Rennes, France. In January 2006, he joined the Universitat Politècnica de Catalunya, Barcelona, Spain, as a Ramn-y-Cajal Researcher, where he is currently an Associate Professor in the area of remote sensing and microwave technology. His research interests include SAR and multidimensional SAR, radar polarimetry, physical parameter inversion, digital signal processing, estimation theory, and harmonic analysis.

Dr. López-Martínez is an Associate Editor of the IEEE JOURNAL OF SELECTED TOPICS IN APPLIED EARTH OBSERVATIONS AND REMOTE SENSING and he served as Guest Editor of the European Association for Signal Processing (EURASIP) Journal on Advances in Signal Processing. He has organized different invited sessions in international conferences on radar and SAR polarimetry. He has presented advanced courses and seminars on radar polarimetry to a wide range of organizations and events. He received the Student Prize Paper Award at the European Conference on Synthetic Aperture Radar (EUSAR) 2002 Conference and co-authored the paper awarded with the First Place Student Paper Award at the EUSAR 2012 Conference.

Luca Pipia received the B.S. degree (*cum laude*) in electrical engineering from the Università Degli Studi di Cagliari, Cagliari, Italy, in 2002, and the Ph.D. degree in polarimetric differential SAR interferometry (PolDIInSAR) from the Universitat Politècnica de Catalunya (UPC), Barcelona, Spain, in 2009.

From June 2001 to December 2001, he was with the High-Frequency Institute of the German Aerospace Center (DLR), Oberpfaffenhofen, Germany, where he worked on land classification using polarimetric SAR (PolSAR) information. From 2003 to 2009, he was with the Remote Sensing Laboratory, Departament de Teoria del Senyal i Comunicacions, UPC, where he was deeply involved in the development and assessment of a novel polarimetric formulation of coherence-based advanced DinSAR techniques using real ground-based PolSAR data. Currently, he is with the Remote Sensing Group, Institut Cartogrfic de Catalunya. His research interests include SAR polarimetry, differential SAR interferometry, and the retrieval of quantitative information from hyperspectral visible, near- and thermal-infrared airborne data.

Dr. Pipia has served as a Reviewer for the IEEE JOURNAL OF SELECTED TOPICS IN APPLIED EARTH OBSERVATIONS AND REMOTE SENSING, the IEEE GEOSCIENCE AND REMOTE SENSING LETTERS, and the IEEE TRANSACTIONS ON GEOSCIENCE AND REMOTE SENSING.

Ground-Based Polarimetric SAR Interferometry for the Monitoring of Terrain Displacement Phenomena. Part II: Applications

Rubén Iglesias, *Student Member, IEEE*, Albert Aguasca, *Member, IEEE*, Xavier Fabregas, *Member, IEEE*, Jordi J. Mallorqui, *Senior Member, IEEE*, Dani Monells, *Student Member, IEEE*, Carlos López-Martínez, *Senior Member, IEEE*, and Luca Pipia

***Abstract*—Urban subsidence and landslides are among the greatest hazards for people and infrastructure safety and they require an especial attention to reduce their associated risks. In this framework, ground-based synthetic aperture radar (SAR) interferometry (GB-InSAR) represents a cost-effective solution for the precise monitoring of displacements. This work presents the application of GB-InSAR techniques, particularly with the RiskSAR sensor and its processing chain developed by the Remote Sensing Laboratory (RSLab) of the Universitat Politècnica de Catalunya (UPC), for the monitoring of two different types of ground displacement. An example of urban subsidence monitoring over the village of *Sallent*, northeastern of Spain, and an example of landslide monitoring in *El Forn de Canillo*, located in the Andorran Pyrenees, are presented. In this framework, the key processing particularities for each case are deeply analyzed and discussed. The linear displacement maps and time series for both scenarios are showed and compared with in-field data. For the study, fully polarimetric data acquired at X-band with a zero-baseline configuration are employed in both scenarios. The displacement results obtained demonstrate the capabilities of GB-SAR sensors for the precise monitoring of ground displacement phenomena.**

***Index Terms*—Differential synthetic aperture radar (SAR) interferometry (DInSAR), displacement monitoring, ground-based SAR (GB-SAR), frequency modulated continuous wave (FMCW) radar, ground-based SAR interferometry (GBInSAR), persistent scatterer interferometry (PSI), polarimetric SAR interferometry (PolInSAR), steepest linear frequency modulated continuous wave (SLFMCW) radar.**

I. Introduction

THE DEVELOPMENT of differential synthetic aperture radar (SAR) interferometry (DInSAR) algorithms during the last decade has demonstrated their usefulness for the precise monitoring of ground displacement episodes [1], [2] with millimetric precisions [3]. Furthermore, DInSAR algorithms have boosted the development of persistent scatterer interferometry (PSI) techniques which allows obtaining not only accurate linear velocity estimations but also time series containing the nonlinear displacement component of affected areas [4]–[15].

In this context, two different kinds of sensors may be considered: orbital/airborne or ground-based. Spaceborne SAR sensors have demonstrated to be extremely successful for studying the evolution of displacement processes, especially, over wide areas. Despite this, when flexibility in terms of revisiting time or sensor orientation toward the scene is required, orbital sensors cannot fulfill the requirements. Airborne sensors represent a more flexible solution but contrarily the data processing becomes more difficult. Furthermore, the monitoring campaigns are generally costly and complex to carry out. For this reason, the research activity of several groups has been recently addressed to the development of terrestrial SAR systems [16], [17]. Flexible, easy to deploy, and cheaper if compared to space- or airborne solutions, Ground-Based SAR (GB-SAR) sensors can be presented as an effective, and sometimes complementary, solution for the precise monitoring of small-scale phenomena [18]–[33].

Due to the capability of GB-SAR sensors to carry out a *quasi* continuous monitoring, one of their most relevant application corresponds to the slope monitoring of open pit mines, in which such systems potentially work as an Early Warning System (EWS) [34]–[37]. Other relevant applications include slope instability monitoring related to rock-slides [38], [39], [21], volcanoes [40], urban monitoring [41]–[43], structure monitoring [44], [16], dike monitoring [45], glacier monitoring [46], and landslides [43], [45], [47]–[50]. A complete classification of the different GB-SAR applications can be found in [51].

This paper presents the applicability of the RiskSAR GB-SAR sensor, developed in the Remote Sensing Laboratory (RSLab) of the Universitat Politècnica de Catalunya (UPC) and widely described in Part I of this paper [52], for the efficient monitoring of ground displacement phenomena.

The RiskSAR sensor [22], [29] is based on the employment of high-rate steepest linear frequency modulated continuous wave (SLFMCW) signals. This type of solution allows performing faster scans compared with vector network analyzer (VNA)-based solutions and, hence, minimize the impact of

Manuscript received March 31, 2014; revised July 22, 2014; accepted September 18, 2014. This work was supported in part by the Big Risk Project (contract number BIA2008-06614), and in part by the Project TEC2011-28201-C02-01 funded by the Spanish MICINN and FEDER funds.

R. Iglesias, A. Aguasca, X. Fabegas, J. J. Mallorqui, D. Monells, and C. López-Martínez are with the Department of Signal Theory and Communications, Universitat Politècnica de Catalunya, 08034 Barcelona, Spain (e-mail: ruben.iglesias@tsc.upc.edu; aguasca@tsc.upc.edu; fabregas@tsc.upc.edu; mallorqui@tsc.upc.edu; dmonells@tsc.upc.edu; carlos.lopez@tsc.upc.edu).

L. Pipia is with the Institut Cartogràfic Geològic de Catalunya, 08038 Barcelona, Spain (e-mail: luca.pipia@icc.cat).

Color versions of one or more of the figures in this paper are available online at http://ieeexplore.ieee.org.

Digital Object Identifier 10.1109/JSTARS.2014.2366711

tropospheric disturbances and target instabilities during the scanning time. This radar architecture also favors obtaining reliable polarimetric SAR (PolSAR) measurements with no dramatic increase in the scanning time. In this context, it has been recently demonstrated that polarimetric SAR interferometry (PolInSAR) techniques outperform classical single-polarization PSI performance [53]–[55].

The applications shown in this work are focused on the GB-SAR sensor working in a discontinuous operation mode, which means revisiting the site during different measurement days with a certain temporal span. This can be applied when the deformation process is slow enough and does not require a continuous monitoring. As widely explained in [52], the processing for this configuration mode consists of performing first a temporal averaging of each daily data set. This is referred to as short-term processing (STP) and allows improving the signal-to-noise ratio (SNR) of time-stationary targets, leading to a time-averaged SLC image for each measurement day. In the following step, referred to as long-term processing (LTP), the atmospheric artifacts among the different time-averaged SLC images are compensated for. From all methods available in the literature, the RiskSAR processing chain makes use of model-based solutions to carry out the atmospheric phase screen (APS) compensation. This kind of solution has proven to be very effective since it reaches very good results with no need of extra meteorological data or stable ground control points (GCP). Carrying out a proper APS estimation and compensation process is mandatory in order to obtain reliable displacement map estimations. Once a set of APS-free interferograms are obtained, PSI techniques can be applied to obtain reliable linear and nonlinear estimations of ground displacements. Among all the PSI techniques developed in the last decade, this work focuses on the adaptation of the coherent pixels technique (CPT) to work with zero-baseline data [52].

The linear displacement maps and time series over two very different scenarios, a district affected by subsidence due to the mining activity carried out in the surrounding area during the last century, and an active slow-moving landslide located in a mountainous region, are presented. The main logistics and processing particularities for each case are widely discussed. In both scenarios, the RiskSAR sensor was operated at X-band due to its excellent tradeoff among the high spatial resolution of the SLC images acquired, the possibility to achieve a reliable APS compensation and a fine sensitivity to ground displacements. For this reason, the RiskSAR sensor is referred to as RiskSAR-X hereinafter. The slant-range resolution working at X-band is 1.25 m. The cross-range resolution is on the order of 10 mrad, ranging from 0.75 m at near range up to roughly 5 m at a far range of 1500 m. In both cases, the processing is benefited from the use of fully polarimetric data.

The paper is organized as follows. Section II refers to GB-SAR measurement logistics, with emphasis in the importance of choosing a correct location for the sensor depending on the nature of the scenario and on the ground displacement process characteristics. Sections III and IV present the zero-baseline PSI results in the urban scenario of *Sallent* and in the landslide of *El Forn de Canillo*, respectively. The main conclusion and major remarks are given in Section V.

II. Measurement Logistics

Once a GB-SAR solution is adopted for the monitoring of a certain area, the location of the sensor constitutes a crucial issue in order to maximize the performance of the technique. In addition to be able to cover the whole area of interest, two important aspects must be taken into account: the minimization of the so-called SAR geometrical distortions (foreshortening, layover, or shadowing) to have the regions of interest visible to the radar, and the maximization of the sensor sensitivity to deformation, as SAR systems are only able of detecting displacements in the line-of-sight (LOS) direction. The selection of the adequate emplacement helps to maximize the sensitivity of the interferometric phase to the deformation process to monitor, and thus provide the best results possible.

These aspects must be taken into account when planning the measurements and, furthermore, in the final interpretation of the results. This section presents their analysis in order to maximize the performance of ground-based SAR interferometry (GB-InSAR) techniques depending on the nature and environmental conditions of the displacement phenomenon.

A. Minimization of SAR Geometric Distortion Effects

Regardless of the platform nature, three geometric distortions are present in SAR imaging. These are the foreshortening, the layover, and the shadowing [56]. Unlike orbital-based SAR sensors, which are constrained by the orbit geometry, GB-SAR sensors allow fitting the sensor location and orientation to the specific characteristics of the area under study. This fact allows to minimize, or at least control, these distortion effects.

Shadowing must be especially taken into account when facing urban monitoring applications. Urbanized areas are typically characterized by having a relatively large number of tall man-made structures, such as buildings. If the location of the sensor is decided without considering its impact, it can lead to a large number of shaded areas in the SAR acquisitions. The location of the instrument at a certain height in order to achieve a top view of the area under study minimizes shadowing impact.

Contrarily, landslide areas are typically characterized by having a low numbers of man-made structures. Therefore, shadowing has less impact in these applications. Despite this, it is important to choose a location which allows overcoming the geographical accidents of the scenario. In these areas, foreshortening plays a more critical role. The illumination angle must depart from the local slope to avoid as much as possible the compression effect produced by this geometrical distortion. A good strategy consists of locating the instrument at the base of the hillside, some meters away from the slope, in order to illuminate all the area of interest minimizing the shadowing and the foreshortening artifacts.

B. Maximization of the Sensitivity to Deformation

As stated above, SAR systems only have sensitivity in the LOS direction. Due to its different orientation, the measured

displacements are, in general, not the real ones but a projection of them. Using a vector notation, both can be defined as

$$\mathbf{V}_{LOS} = |\mathbf{V_{LOS}}| \cdot \widehat{\mathbf{l}}_{\mathbf{LOS}}$$
$$\mathbf{V}_{G} = |\mathbf{V_G}| \cdot \widehat{\mathbf{l}}_{\mathbf{G}} \quad (1)$$

where $\mathbf{V}_G$ is the ground displacement vector, this is the real deformation, and $\mathbf{V}_{LOS}$ is the LOS displacement vector, this is the projection. The magnitudes $|\mathbf{V_{LOS}}|$ and $|\mathbf{V_G}|$ are related to the intensity of the displacement, and the unitary vectors $\widehat{\mathbf{l}}_{\mathbf{LOS}}$ and $\widehat{\mathbf{l}}_{\mathbf{G}}$ indicate the displacement direction. In fact, the former is only a projection of the latter. Thus, the magnitude of both displacement vectors can be related through a scalar product as follows:

$$|\mathbf{V_{LOS}}| = |\mathbf{V_G}| \cdot \cos(\alpha) \quad (2)$$

where

$$\cos(\alpha) = \widehat{\mathbf{l}}_{\mathbf{LOS}} \cdot \widehat{\mathbf{l}}_{\mathbf{G}} \quad (3)$$

being α the angle between the unitary vectors.

When the ground displacement is expected to be vertical, as it normally occurs with subsidence phenomena in urban scenarios, α directly becomes the local incidence angle θ_{inc}. In this context, higher sensor location elevations over the area of interest imply shorter incidence angles and thus a better sensitivity to the ground displacement.

When facing landslide monitoring the problem becomes more complex as the real motion of a particular point has an intrinsic topographic dependence related with its local slope. With no *a priori* knowledge, the more realistic kinetic model of the displacement direction $\widehat{\mathbf{l}}_{\mathbf{G}}$ is based on considering that the surface mostly moves along the steepest gradient of the terrain slope. This information may be derived employing a digital elevation model (DEM) of the area. Then, the angle α is directly obtained through (3).

For the current polar-orbiting SAR satellites, the look direction is close to East or West, for ascending or descending orbits, respectively. For this reason, spaceborne SAR systems are mainly sensitive to movements along slopes facing either East or West and almost insensitive to movements in North or South directions. In this context, GB-SAR sensors present a potential advantage with respect to spaceborne ones since they are not constrained by any orbit geometry. GB-SAR sensors can be placed at an adequate location and fit their orientation for illuminating a specific site according to the geometry of the problem.

A good strategy in landslide monitoring applications consists of locating the instrument at the foot of the hillside, using an illumination angle facing the down-slope direction in order to maximize the displacement detection.

III. Urban Monitoring Study Case

Urban monitoring represents one of the most interesting issues and major research topics in the SAR community. Subsidence hazards in urban areas involve from damage in man-made structures to the sudden collapse of entire neighborhoods, thus endangering human lives. Two surveying methods are mainly used for ground deformation monitoring purposes over urban scenarios. These are leveling and global positioning system (GPS). In most cases, the difficulty to cover large areas and the poor densities of measurements provided by these techniques hinder the effective identification and characterization of complex deformation episodes. Geotechnical devices such as inclinometers, extensometers, or piezometers present similar drawbacks.

GB-SAR sensors hence represent a useful alternative with respect to the previous surveying techniques. They provide precise estimations of ground displacement phenomena over larger areas with a high density of measures at a lower cost.

This section presents the study case of a linear urban subsidence phenomenon produced in a district affected by the former mining activity carried out around the area.

A. Test Site and Data Set

The test site selected corresponds to a district known as *El Barri de l'Estació*, located in the village of *Sallent*, northeastern Spain. Nowadays, there is a subsidence phenomenon induced by the intense mining activity carried out in the area during the second quarter of the last century. This deformation process is the consequence of the exploitation of the *Enrique Mine*, which was opened from 1932 to 1973 and reached a maximum depth of 260 m.

Unexpectedly, during the intense mining works of 1954, a natural cavity of about 120 m high and 40 m wide was found. Some years later, during 1957 and 1962, several floods from the *Llobregat River* occurred that made difficult to continue with the mine exploitation, and finally leading to the closure of the *Enrique Mine* in the year 1973.

During the period of abandoning, the mine was filled up with saturated salty water. Some decades after, in 1990s, heavy damages started to be appreciated in several man-made structures built within the affected district of *El Barri de l'Estació* [see Fig. 1(a)].

As a response to the problem, the administration started a research program to identify, characterize, and model the subsidence phenomena observed in the affected area [57]. A multiple set of techniques such as laser topographic leveling, geological mapping, geophysical prospection, extensometric measurements, and drilling was employed to evaluate the risk of the already weakened structures to collapse.

In this framework, the RSLab group, jointly with the Institut Cartogràfic i Geològic de Catalunya (ICGC), started in 2003, the study of this area with PSI techniques using spaceborne acquisitions of the European Remote Sensing (ERS) satellite [58]. A new collaboration between the RSLab and the ICGC started in 2006 to assess the performance of GB-SAR sensors in such scenarios. A 1-year measurement campaign was carried out using the RiskSAR-X sensor [22], [29]. It started in June 2006 and finished in March 2007. GB-SAR data were acquired during nine measurement days, as reported in Table I. In each measurement day, several scans were carried out in order to improve the SNR of measures.

(a) (b) (c)

F1:1 Fig. 1. (a) Example of the heavy damages observed in *El Barri de l'Estació*, *Sallent*. (b) Picture of the *El Barri de l'Estació* observed from the (c) RiskSAR point
F1:2 of view.

T1:1 TABLE I
T1:2 TIMETABLE OF SALLENT MEASUREMENT DAYS

Campaign	Date dd/mm/yyyy	Start Time hh:mm	Stop Time hh:mm	Numb. of Scans
1	29/06/2006	11:00	16:00	27
2	26/07/2006	08:00	11:30	30
3	19/08/2006	10:40	16:00	39
4	20/10/2006	09:40	15:00	31
5	14/11/2006	12:30	16:30	41
6	28/11/2006	19:00	08:40	44
7	18/12/2006	20:45	05:00	49
8	13/02/2007	22:00	09:55	37
9	14/03/2007	20:00	09:50	41

B. System Setup

As seen in Section II, in urban monitoring applications, the GB-SAR location must minimize as far as possible the effects produced by the buildings present in the scenario. This implies to select an emplacement as high as possible in order to have a top view of the area of interest, which minimizes the shadowing and maximizes the sensitivity to vertical displacements.

For these reasons, the instrument was finally installed on the top of a cliff of 84 m height, 200 m away in the range direction from the district *El Barri de l'Estació*. This location provided an incidence angle varying from 72° up to 82°. It is worth pointing out that installing the radar on the cliff's border prevented the radar front-end of saturations caused by close targets. Moreover, the system was placed on a base at approximately 30 cm above the ground to raise the rail and reduce the impact of the nearby vegetation.

Another important issue was to ensure a millimetric repositioning of the instrument to avoid a later coregistration of the data. In order to guarantee the repeatability of the observation conditions, the system was mounted over a cement base reinforced with a lightweight metallic frame. A picture of the RiskSAR-X point of view, and the final system setup is detailed in Fig. 1(b) and (c), respectively.

The area of interest illuminated by the RiskSAR sensor extended to approximately 400 m in range and 300 m in width. Each scan took roughly 2.5 min to perform a fully polarimetric measure.

C. Short-Term and Long-Term Processing

Prior to the application of the zero-baseline CPT algorithm to obtain PSI results, some important aspects about the STP and LTP [52] processing should be briefly remarked.

As seen, *El Barri de l'Estació* is an urban area plenty of man-made structures. For this reason, the reflectivity image of the region covered by the sensor has a large dynamic range, with strong reflectivity peaks corresponding to man-made structures, see Fig. 2(a). The coherence in these scenarios remains very high along the temporal axis, as illustrated in Fig. 2(b) and (c), which shows the coherence maps from two acquisitions with a temporal baseline of 15 min and 23 days, respectively. As shown, the highest coherence pixels are preserved in those areas with higher reflectivity, coinciding with the man-made structures present in the scenario. This fact is of crucial importance, since it will lead to a robust network of temporally coherent scatterers in the later PSI processing.

As it is detailed in [52], in addition to the thermal noise and the temporal decorrelation phenomena, APS represents the most relevant distortion artifact on the interferometric phase. It directly impacts in the STP, which aims to obtain a reliable high-quality time-averaged image from each measurement day. In addition, it also affects the LTP, whose objective is obtaining a collection of APS-free interferograms for the later PSI processing. From all the available methods, the RiskSAR sensor makes use of model-based solutions [59], [60] since they proved to be very successful with no extra meteorological data or stable GCP.

Fig. 2(d)–(f) shows the interferometric phase evolution due to APS between images separated by temporal spans of 15 min, 1 h, and 4 h, respectively. In such regions, the atmospheric artifacts are smooth in both the spatial and temporal domains. The linear approximation proposed in [59] is sufficient to deal with the APS problematic in these scenarios with soft topography [52].

In order to illustrate the good performance of APS model-based solutions in urban scenarios, the compensation process of an interferogram with a temporal span of 2 h is presented in Fig. 3. With the goal of generating a reliable vector of observations to carry out the linear regression, only the points with the highest coherence values ($\gamma > 0.95$) are employed. In order to estimate the coherence a 9×9 multilook is selected. Black dots represent the projection onto the range axis of the interferometric phase. Notice how, as expected, the interferometric phase

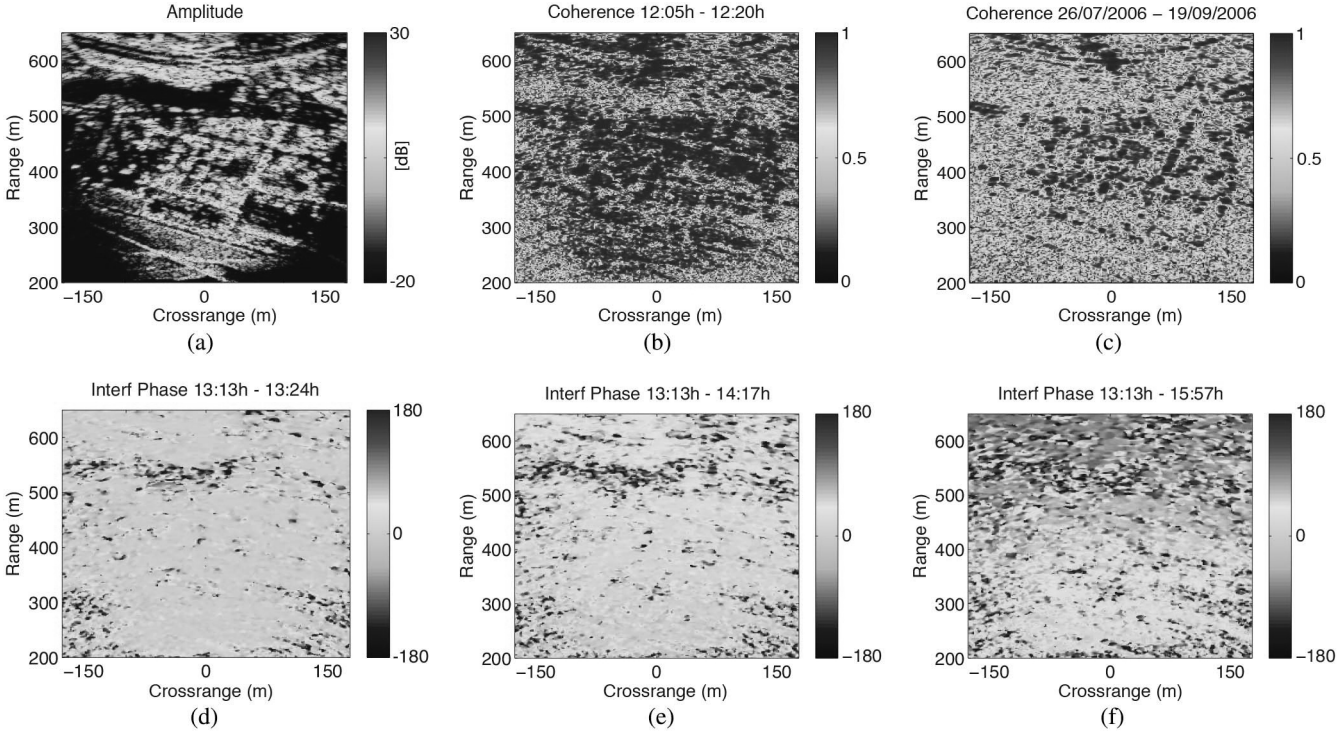

F2:1 Fig. 2. (a) Reflectivity image in dB and coherence maps between acquisitions with a temporal baseline of (b) 15 min and (c) 23 days corresponding to the area of
F2:2 *El Barri de l'Estació*, *Sallent*. Interferometric phase due to the APS between images separated in time (d) 15 min (e) 1 h, and (f) 4 h approximately.

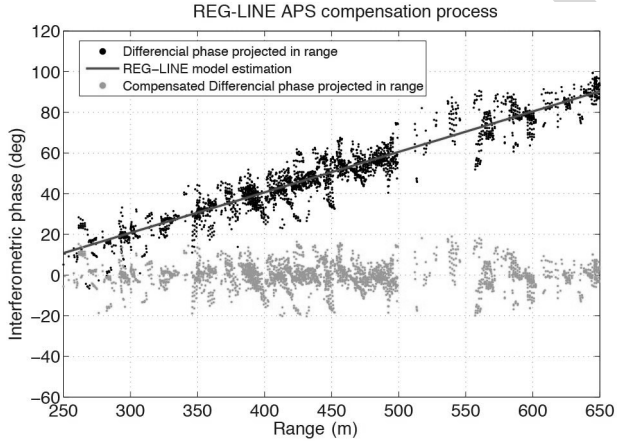

F3:1 Fig. 3. Compensation process of an interferogram with a temporal span of 2 h
F3:2 over those points with a coherence value over 0.95. Black dots represent the
F3:3 projection of the interferometric phase onto the range axis. Red line accounts
F3:4 for the estimated APS using a linear regression. Green dots correspond to the
F3:5 interferometric phase once it has been compensated for.

exhibits a strong linear behavior in the range direction. The red line represents the estimated APS using the linear regression method indicated in [52] and [59]. Finally, the green dots correspond to the compensated interferometric phase. Notice how the final interferometric phase has a mean value close to zero. This value is normal since during this short temporal span the interferometric phase may be considered totally independent of any deformation process. In other words, within the same measurement day no detectable movements are expected. Indeed, the interferometric phase of APS-free interferograms has a mean value close to zero.

Due to the large number of high-coherent scatterers available in urban scenarios, the basis-based method explained in [52], which uses a set short-time compensation functions between consecutive daily temporal-averaged images, is not required. Exploiting polarimetry at this point is not necessary for the same reason as well.

Finally, in order to reduce the effects of urban target short-time instability induced by human activities, the sample selection technique proposed in [61] is employed for the generation of time-averaged SLC images. The detection of the long-term polarimetric behavior providing the highest number of samples for each day of measurements guaranteed a higher quality of the final interferometric phase information.

D. Displacement Results

The displacement map retrieval process is carried out with the zero-baseline adaptation of the CPT algorithm [52]. The choice of the pixel selection method depends on the number of acquisitions at disposal and on the nature of the scatterers to detect, either distributed or point-like scatterers. For this case, since the number of images available is short, only 9, the coherence stability criterion has demonstrated to perform well. A threshold of mean coherence corresponding to 0.7, which is equivalent to a phase standard deviation of about $15°$, with a 5×5 multilook window [62], has been established in order to filter out the noisy pixels from the processing. In this type of urban scenarios, a 5×5 multilook window has demonstrated a good performance to detect man-made structures.

At this point, the processing has been benefited by the use of polarimetric optimization techniques [52]. In particular,

the equal scattering mechanism (ESM) polarimetric optimization method [54] has been selected to improve the quality of interferograms. This is translated in roughly a twofold increase in the number of pixels during the pixel selection step.

Finally, the linear velocity map retrieved using the zero-baseline CPT technique is projected over the vertical as indicated in Section II.

The PSI results obtained with the RiskSAR-X sensor are compared with the results provided by the experts of the ICGC [see Fig. 4(a) and (b)], respectively. On the hand, the ground-truth information was obtained by means of a continuous laser topographic levelling system that monitored a set of positions, indicated as dots in Fig. 4(b), during the same period of the GB-SAR campaign. This discrete set of measurements has been employed to obtain the result provided in the same figure through interpolation. On the other hand, due to the high number of high-coherent pixels in the area, GB-SAR results have also been interpolated in order to ease the comparison with the ground-truth available. A high agreement concerning the spatial description of the deformation process may be observed between both techniques. Notice how the position of the area characterized by the maximum deformation bowl perfectly matches. Despite this, it must be pointed out that GB-SAR measurements lead to a slight overestimation of the displacement rate in the center of the deformation focus, 5 cm/year against the 4.5 cm/year given by the *in situ* ground-truth measurements. The difficulty to install the instrument at a higher elevation, to reach shorter incidence angles and maximize the detection in the LOS direction, could explain this slight discrepancy.

Fig. 4(c) shows the time series of a coherent scatter located in the maximum deformation bowl of the area. A strong linearity, as expected from ground-truth measurements and from the spaceborne results available [57], [58], may be observed.

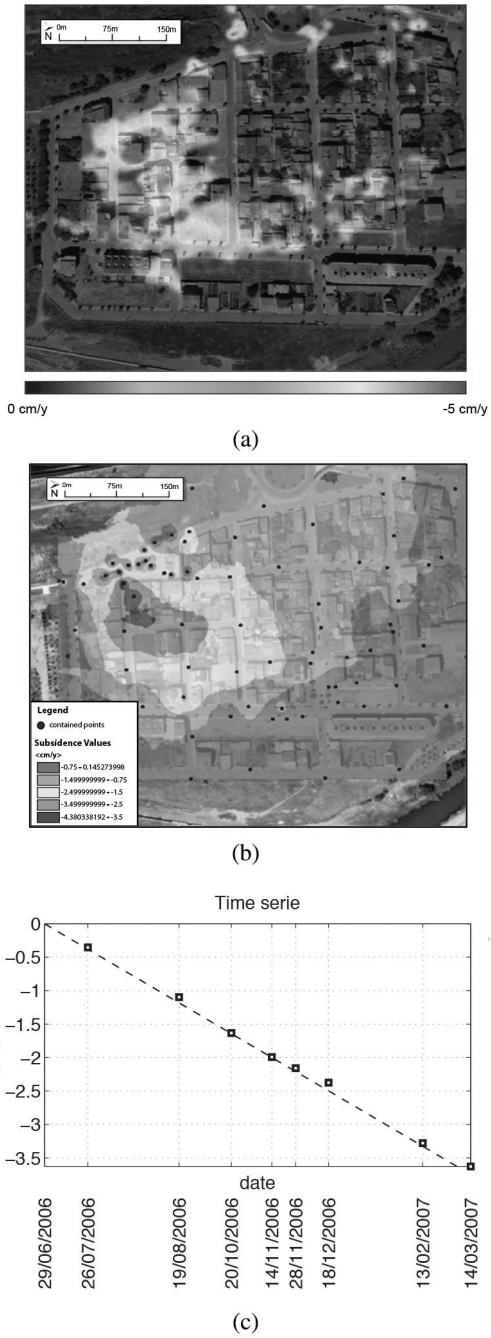

Fig. 4. (a) Vertical linear displacement map retrieved by using the zero-baseline CPT algorithm. (b) Ground-truth map provided by the ICGC employing laser topographic leveling techniques. (c) Displacement time series of a point located in the center of the deformation focus with a linear velocity of 4.7 cm/year. F4:1 F4:2 F4:3 F4:4

IV. Landslide Monitoring Study Case

Due to the all-weather and day-night capability to accurately detect ground and surface deformations, GB-InSAR has become a useful tool for geo-hazard assessment during the last few years. The accurate monitoring of landslide surfaces represents an important issue in order to achieve a better understanding of landslide mechanisms, and detecting its potential risks to ensure the safety of people living in such areas.

Traditionally, landslide monitoring has been carried out employing different geotechnical devices, including inclinometers, extensometers, piezometers, and GPS differential networks. These in-field measurements present, in general, a benchmark density and a lower extent compared with SAR techniques. In addition, they require the installation of devices directly onto the landslide surface, which can be a problem when the accessibility to the area is complex. The development of remote sensing monitoring tools based on SAR data is becoming an important issue for many authorities in order to ensure the safety of people living in such areas.

A. Test Site and Data Set

The test site selected to demonstrate the applicability of GB-SAR sensors in these applications corresponds to the landslide of *El Forn de Canillo*, located in the Andorran Pyrenees. It has been widely studied since 1980s, and today it is considered as one of the largest landslides of the Pyrenean region [see Fig. 5(a)].

The landslide is composed by a sequence of slides and earthflows with a complex structure, which affects an estimated mass

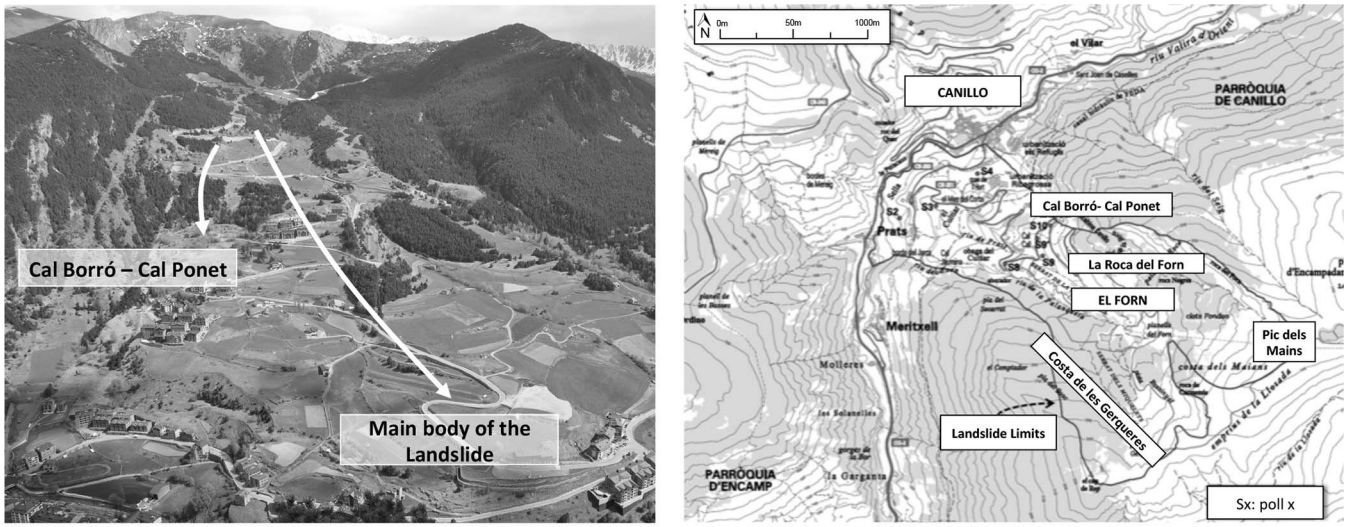

(a) (b)

F5:1 Fig. 5. (a) General overview of the landslide of *El Forn de Canillo*. (b) Landslide limits and location of the devices installed.

at around $300\ \mathrm{Mm}^3$. In this context, three major sliding units were identified in 1994 [63]. The first one corresponds to a slide originated in the area of *Pla del Géspit-Costa de les Gerqueres* [Fig. 5(b)], located in the south-west of the landslide, which reached the foot of the hillside. A second unit was originated under *El Pic de Maians* [see Fig. 5(b)] reaching a height of 1640 m, and that overlaps with the previous sliding unit, closing in the *Valira River* valley. Finally, a new rotational slide with a lower extension originated on the hillside known as *La Roca del Forn* [see Fig. 5(b)] in the north-east side of the hillside has been identified.

The landslide of *El Forn de Canillo* was originated as the result of the hillside destabilization, due to a decompression phenomenon after the removal of the *Valira Glacier*, between 13 000 and 16 000 years before present [63]. The *Valira River* has been progressively eroding the base of the whole mass without reaching the bedrock, and thus originating the landslide.

The geological observations accumulated during the last decades have evidenced the presence of a main slide mass with a residual movement of some millimeters per year, accompanied by a local failure in the area known as *Cal-Ponet Cal-Borró* [see Fig. 5(b)] within the third slide unit described above. This slide is presenting today a major activity coinciding with periods of strong rainfalls and snow melting.

In front of all these evidences, the authorities promoted several actions in the year 2000 for the management of the risk related with the geo-hazard threats associated with landslides, rockfalls, and debris flows in the Andorran Pyrenees. Some specific management plans were carried out for the monitoring of *El Forn de Canillo*.

Between 2007 and 2009, a complex network of geotechnical devices, including inclinometers, rod extensometers, and piezometers, was installed in order to characterize and understand the dynamics of the landslide. A total of 10 boreholes, referred from *S1* to *S10* in Fig. 5(b), reaching a depth between 40 and 60 m, were drilled and equipped with this instrumentation. The measurements provided by these devices have been recently studied with the objective of locating the sliding surfaces and characterizing the displaced material [64].

Unfortunately, some of the boreholes did not reach the needed depth, and consequently the installed devices did not work properly in some points. Despite this, as it has been expected from *in situ* observations, the installed devices evidenced that, in addition to a residual movement of the main lobe of some millimeters per year, the most active part of the landslide corresponds to the secondary landslide of *Cal Borró-Cal Ponet*, which between May and June 2009 registered a velocity up to roughly 2 cm/month [64]. Intense rain events and sudden snow melting was observed during this period. As an example, a famous house built in the mid-19th century, located next to the foot of this secondary landslide near to *S10*, has experienced a significant damage [see Fig. 6(a)]. Several cracks and shear openings along the road pavements close to this area have also appeared over the last years [see Fig. 6(b)].

In 2011, the use of GB-InSAR techniques to identify and characterize the dynamics of the landslide were planned. The reasons were twofold: on the hand, most of the geotechnical devices implemented did not work properly providing unreliable measures and, on the other hand, conventional geotechnical field measurements present lower densities and thus a worse coverage compared with SAR techniques. For this reason, the RSLab, in collaboration with the Department of Geotechnical Engineering and Geosciences of the UPC, carried out a 1-year measurement campaign, from October 2010 to October 2011, with the objective of identifying and characterizing the behavior of the landslide.

Since the landslide of *El Forn de Canillo* is nowadays quite stable with some residual movement of the order of few centimeters per year, a continuous monitoring was considered clearly unfruitful. For this reason, a total of 10 daily data sets were collected with a temporal base line of approximately 1 month, performing thus a discontinuous monitoring, sufficient to avoid phase unwrapping (see Table II).

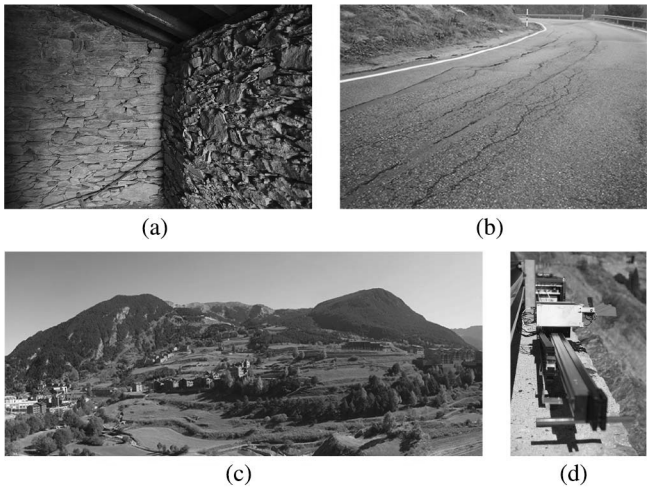

F6:1 Fig. 6. (a) Interior view of the cracked walls of a small farmhouse located in
F6:2 the area of *Cal Borró-Cal Ponet*. The curved shape of the wall indicate the
F6:3 presence of displacements in this area. (b) Cracks and shear openings along a
F6:4 road pavement close to the area of *Cal Borró-Cal Ponet*. (c) Panoramic view of
F6:5 *El Forn de Canillo*, in the Andorran Pyrenees from (d) the RiskSAR point of
F6:6 view.

T2:1 TABLE II
T2:2 TIMETABLE OF EL FORN DE CANILLO MEASUREMENT DAYS

Campaign	Date dd/mm/yyyy	Start Time hh:mm	Stop Time hh:mm	Numb. of Scans
1	21/10/2010	09:57	12:08	15
2	18/11/2010	17:04	19:13	24
3	09/02/2011	17:00	19:48	33
4	07/04/2011	18:17	23:30	60
5	06/05/2011	10:02	11:47	22
6	25/05/2011	16:09	20:08	50
7	09/06/2011	13:20	16:32	51
8	05/07/2011	08:25	12:24	52
9	06/09/2011	11:49	04:05	88
10	05/10/2011	11:57	16:42	66

B. System Setup

The RiskSAR-X sensor was located at the foot of the landslide, 100 m away from the slope, in order to reduce the foreshortening and to maximize the detection of the deformation considering that the landslide moves along the steepest gradient of the terrain slope, as seen in Section II. This emplacement also allows overcoming the geographical accidents of the scenario in order to avoid shadowing in SAR images.

The final area of observation was approximately 500 m in height, 1600 m in range, and 1000 m in width. In addition, as in the urban monitoring case, the system was placed on a base at the height of approximately 30 cm above the ground, to level the rail and avoid the impact of the nearby vegetation in the measurements. As in the previous study case, each scan took roughly 2.5 min to perform a fully polarimetric measure.

A picture of the RiskSAR-X point of view and the sensor's location is detailed in Fig. 6(c) and (d), respectively.

C. Short-Term and Long-Term Processing

Regarding the characteristics of the scenario, *El Forn de Canillo* is mainly covered by vegetation and only contains some man-made structures and few rocky areas suitable to perform a reliable GB-InSAR processing. The reflectivity image of the region covered by the RiskSAR-X sensor is shown in Fig. 7(a). Fig. 7(b) and (c) shows the coherence maps of image pairs with a temporal baseline of 13 min and 6 h, respectively.

Notice how the high-reflectivity areas generally correspond to those pixels with higher coherence values, as expected. These pixels belong to man-made structures, rocky areas, or bare surfaces. Notice also how coherence decreases faster on vegetated areas at X-band, and how only man-made structures or rocky areas remain coherent along time. A considerable loss of coherence in only 6 h can be noticed. Preserving high-coherent pixels along time is a critical issue in these vegetated scenarios, as seen hereinafter.

As in the urban subsidence study case, some important aspects about the STP and LTP [52] processing must remarked prior applying PSI techniques.

Regarding the APS, contrarily to the study case of urban areas seen above, mountainous regions present severe atmospheric phase fluctuations, mainly due to the presence of steep topography. Those regions exhibit strong fluctuations of the atmospheric parameters such as temperature, pressure, and humidity from acquisition to acquisition. Due to this reason, the spatial homogeneity assumption, fulfilled in the previous case, does no longer apply. This fact produces the refractivity index to change in both, the spatial domain, mainly due to the changes in the height, and the temporal one, mainly due to the more extreme atmospheric conditions. The linear-regression model, seen in the urban study case needs to be updated with a second-order term related with the product of range distance and height [52], [60].

In order to illustrate that problem, Fig. 7(d)–(f) is presented. This figure shows the temporal evolution of the interferometric phase after only 1 h. Severe atmospheric phase fluctuations, highly correlated with the steep topography of the scenario, appear in just 1 h leading to over one-cycle phase variations [see Fig. 7(f)].

Fig. 8 shows how the linear-regression model used in the urban study case is not sufficient to compensate for the APS in these scenarios. The compensation process for this example is carried out over an interferogram with a temporal span of only 1 h. The black dots represent the projection of the interferometric phase onto the range axis in the pixels of the image with higher coherence values ($\gamma > 0.95$). Notice how the interferometric phase does no longer exhibit a linear behavior in the range direction. The red line represents the estimated APS using a linear regression, which considerably departs from the interferometric phase, especially at the near and far range. The blue points refer to the new model, indicated in [52] and [60], which accounts for the height of the scenario. Notice how it perfectly fits the interferometric phase trend. Finally, the green dots correspond to the interferometric phase after the compensation process showing the goodness of the proposed technique.

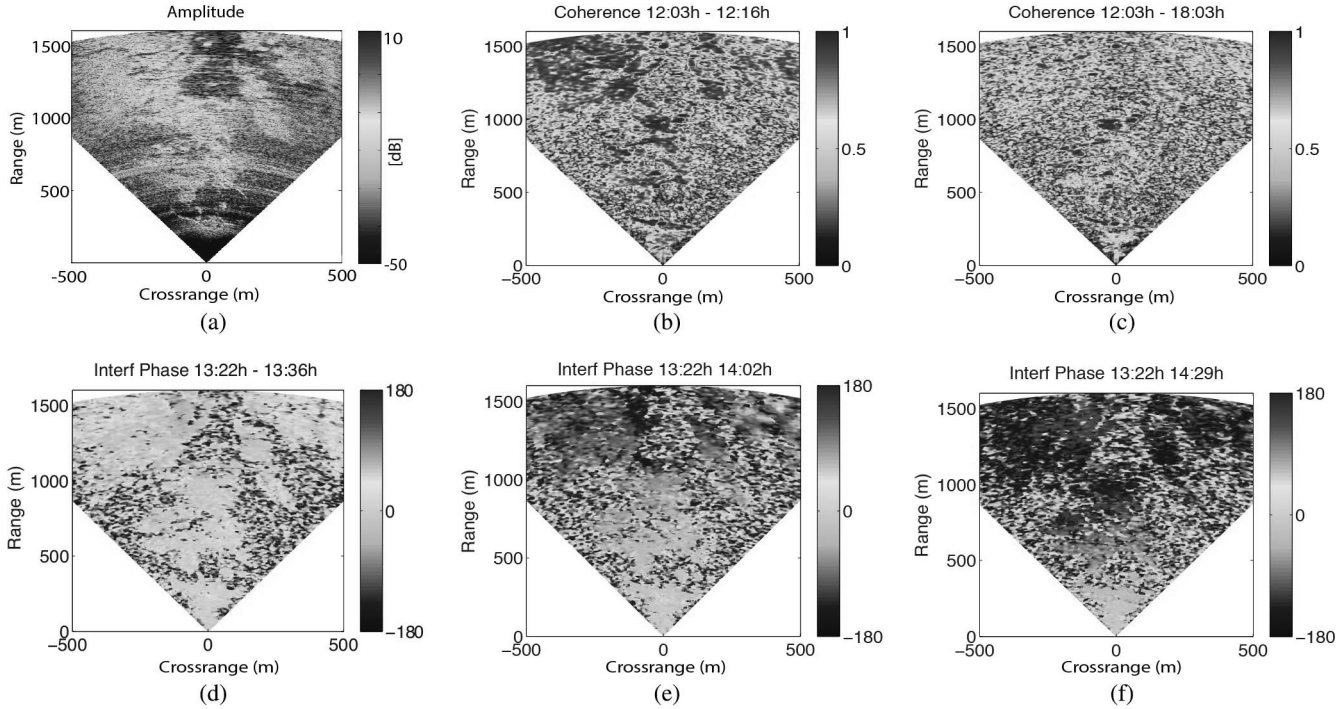

F7:1 Fig. 7. (a) Reflectivity image in dB and coherence maps between acquisitions with a temporal baseline of (b) 13 min and (c) 6 h corresponding to the area of
F7:2 *El Forn de Canillo*, Andorra. Interferometric phase due to APS between images separated in time (d) 15 min (e) 30 min, and (f) 1 h approximately.

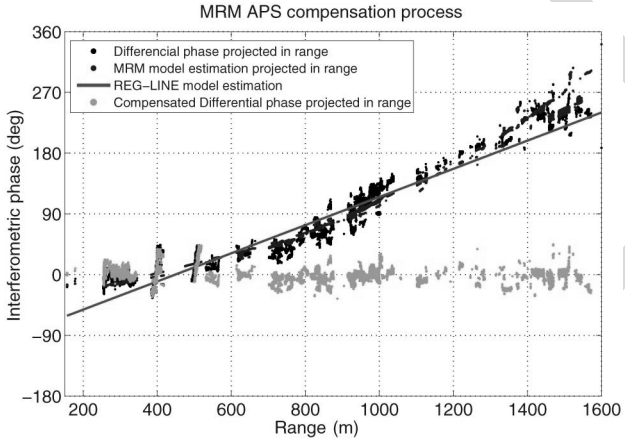

F8:1 Fig. 8. Compensation process of an interferogram with a temporal span of 1 h
F8:2 over those points with a coherence value over 0.95. Black dots represent the
F8:3 projection of the interferometric phase onto the range axis. Red line accounts
F8:4 for the estimated APS using a linear regression. Blue dots refer to the estimated
F8:5 APS using a multiple regression model that takes into account the height of the
F8:6 scenario. Green dots correspond to the interferometric phase once it has been
F8:7 compensated for.

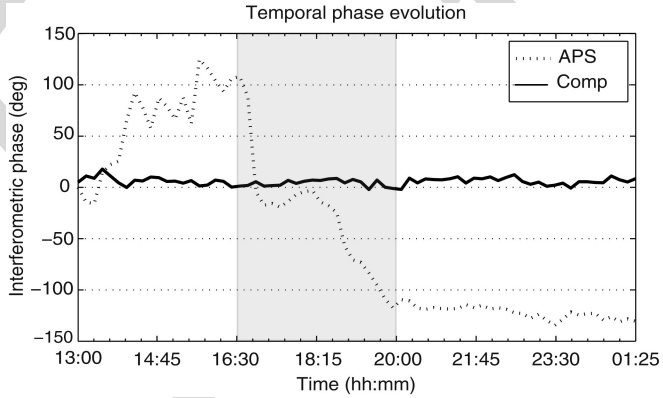

Fig. 9. Phase evolution of a coherent scatterer ($\gamma = 0.97$ using a 9×9 mul- F9:1
tilook) along 70 measures collected during 12 h, from 1:00 P.M. to 1:25 A.M., F9:2
every 10 min. The dotted line refers to the phase evolution before applying the F9:3
APS compensation step. The solid line accounts for the phase evolution once F9:4
the APS is compensated for. The shaded area accounts for the sunset period, F9:5
coinciding with the more severe APS fluctuations. F9:6

Fig. 9 illustrates the good performance of the APS compensation technique along time. This figure presents the phase evolution of a coherent scatterer ($\gamma = 0.97$ using a 9×9 multilook) along a total of 70 measures collected during 12 h, from 1:00 P.M. to 1:25 A.M., every 10 min. The dotted line refers to the phase evolution before applying the APS compensation step meanwhile, the solid one accounts for the phase evolution once the APS is compensated. Since all the measures belong to the same measurement day, it is expected an absence of movement. After performing the APS compensation step, the interferometric phase (solid line) presents a zero-mean value with a low standard deviation value, $\sigma = 3.6°$, which corresponds to 0.16 mm. This experiment demonstrates the good performance of the technique over these kind of scenarios. Fig. 9 also illustrates how the atmosphere fluctuations are more severe during the day, and especially at sunset (shaded area). This fact confirms that the best GB-SAR performances may be achieved measuring at night, especially in these type of mountainous environments.

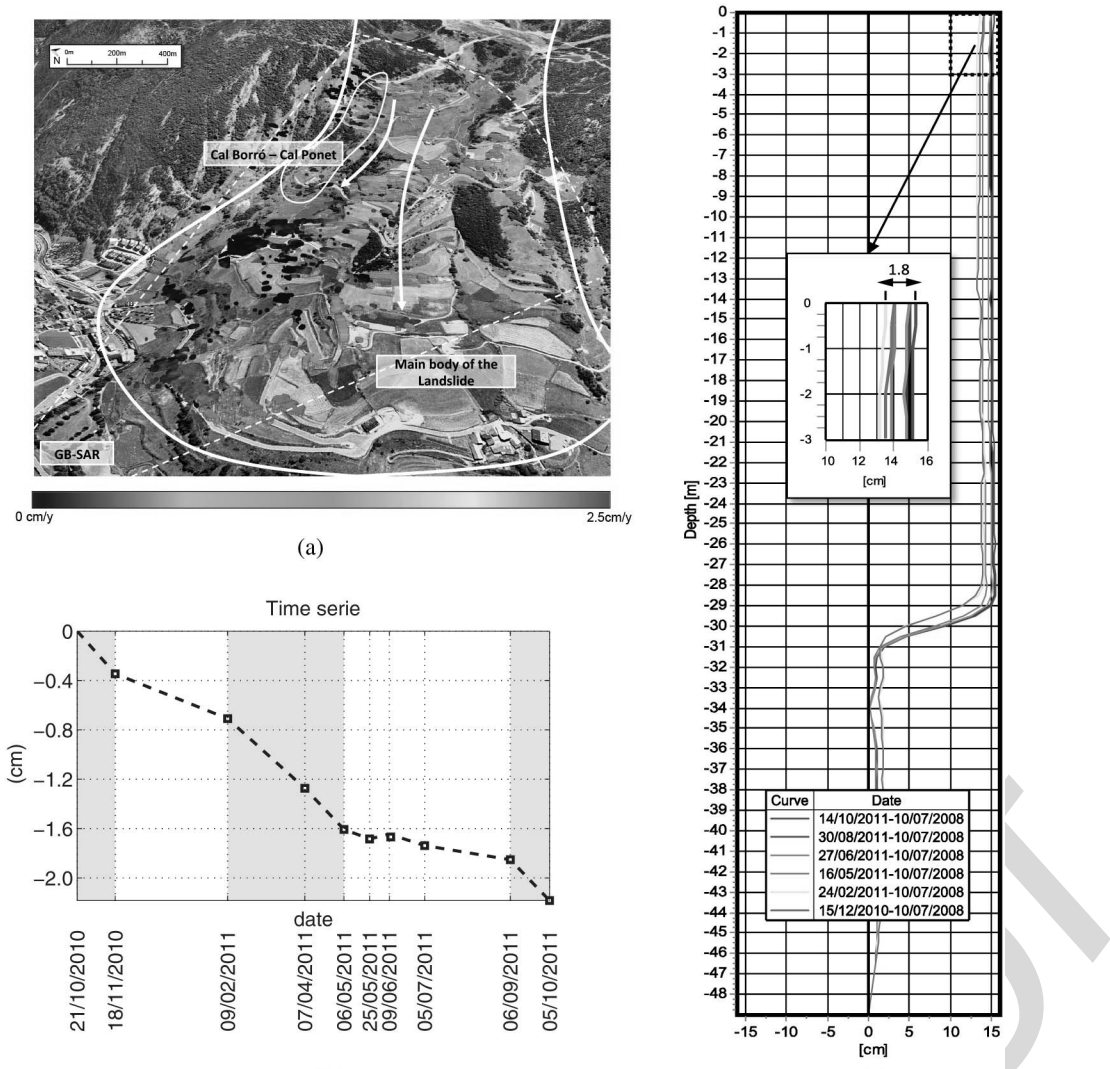

F10:1 Fig. 10. (a) Geocoded down-slope linear ground-displacement of *El Forn de Canillo* obtained with the RiskSAR-X sensor covering the period from October 2010
F10:2 to October 2011. (b) Displacement time series of a point located in the area of *Cal Borró-Cal Ponet* with a linear velocity of $\sim 2.3\,\mathrm{cm/year}$. The shaded areas
F10:3 indicate the periods when the landslide experienced major accelerations. (c) Inclinometric results provided by the firm *Euroconsult* in the borehole *S10*, located in
F10:4 the area of *Cal Borró-Cal Ponet*.

At this stage, maximizing the chances of detecting the major number of coherent scatterers available within the area of study is mandatory.

On the one hand, the LTP has been benefited from the use of the compensating function method described in [52]. This method seeks to perform the APS estimation and compensation process using the shortest temporal baselines available in the data set. A basis of short-term compensation functions between consecutive daily temporal-averaged images, characterized by a minimum loss of coherence are first generated. Then, these are employed to compensate for long-term span interferograms.

On the other hand, the LTP may also be benefited from the use of PolSAR data [52], [60]. A simple strategy, which notably increases the number of coherent scatters selected, consists of selecting for each interferogram which needs to be compensated for, the polarimetric channel providing the highest coherence value. This strategy leads to a twofold increase in the number of high-quality pixels during APS compensation step.

D. Displacement Results

The displacement map retrieval is carried out with the zero-baseline adaptation of the CPT technique [52].

Since the number of images available is short, 10 images, the coherence stability criterion is proposed to carry out the pixel selection. This approach performs well even when a reduced number of images are available. Moreover, this pixel selection criterion has demonstrated to be more suited in natural environments with predominance of distributed scatters.

At this point, since the number of high-quality pixels is smaller for this environment, the zero-baseline CPT algorithm is benefited by the use of a multilayer processing [65].

Two thresholds of mean coherence corresponding to 0.7 and 0.6 are fixed. These correspond to phase standard deviations of about 15° and 20°, respectively, using a 5×5 multilook window [62]. This multilook window maximizes the detection of stable coherent scatters coming from both man-made structures and natural targets, such as rocky areas or bare surfaces.

Furthermore, the ESM polarimetric optimization method [54] has also been employed in order to improve the phase quality of interferograms, and thus achieve a dense network of coherent scatterers to carry out a reliable PSI processing.

Fig. 10(a) shows the final down-slope linear ground-displacement map geocoded over a Google Earth image, using the zero-baseline CPT algorithm. The result shows a high agreement with the conclusions extracted from the field monitoring campaigns made between 2007 and 2009, presented in [64]. Concretely, the displacement map obtained reveals that the main body of the landslide experienced a residual movement of approximately 1 cm/month during the period of observation. In the top-left, part of the hillside a local landslide presenting a higher activity ($\sim 2-2.5$ cm/year) may be appreciated. It corresponds to the so-called secondary landslide of *Cal Borró-Cal Ponet*, described previously. Fig. 10(b) shows the temporal evolution of a high-coherence point belonging to the maximum displacement rate area. Unlike the urban subsidence case studied previously, which was characterized by a strong linear component, the temporal evolution of the displacement has now a strong nonlinear component. It presents several accelerations and stabilizations during the period of measures. The shaded areas in the figure indicate the periods when the landslide experienced major accelerations. Analyzing the figure in detail, it can be observed that the major displacements are produced in the fall (from October to November 2010) and spring (from February to June 2011), coinciding with the major rainfall and snow melting events. In the last period of the graph (September 2011), coinciding again with autumn's arrival, the landslide seems to accelerate again.

Finally, Fig. 10(c) shows the inclinometric results provided by the firm Euroconsult in the borehole *S10*, located in the maximum deformation rate area of *Cal Borr-Cal Ponet*. The figure illustrates a horizontal profile of the deformed shape of the inclinometer casing along the borehole depth in the down-slope direction for different dates. The curves correspond to the period corresponding from December 2010 to October 2011, and all are referred to July 2008. The S-shaped plot reflects that the main shear band is located about 30 m under the surface of the landslide. In order to ease the comparison of the inclinometric results with the ones obtained with the GB-SAR sensor, the upper part of the plot has been amplified. Since the inclinometric results are given in an horizontal plane, these must be divided by the cosine of the slope angle at *S10* ($\sim 20^\circ$) in order to obtain the total down-slope displacement. Notice how during the period from December 2012 to October 2013, the movement along the maximum-slope according to the inclinometer is $\sim 1.8\,\mathrm{cm}/\cos(20^\circ) = 1.91\,\mathrm{cm}$. This corresponds to roughly ~ 2.3 cm/year. Results provided by the GB-SAR are ~ 2.5 cm/year in this area showing a high agreement with the ground truth provided, and demonstrating again the good performance of GB-SAR sensors for the study of ground displacement monitoring applications.

V. Conclusion

Urban subsidence and landslide instabilities involve a wide range of issues that are of concern to governments at all levels. Increasingly, authorities are promoting actions when they threaten public or private properties and, especially, human life, in order to mitigate the socioeconomic losses derived from these problems.

This paper seeks to demonstrate the usefulness of GB-InSAR and PSI techniques, for the monitoring of different kinds of ground displacement phenomena. With this purpose, two different scenarios have been monitored using the RiskSAR sensor and the GB-InSAR processing chain developed by the RSLab [52]. One is an urban area affected by mining induced subsidence and the other a mountainous landslide. For both cases, the obtained deformation maps have been validated with in-field ground-truth data. In addition, the key logistics' particularities and processing approach have been deeply analyzed depending on the nature of the area and the ground displacement process to be monitored. Concretely, the APS estimation and compensation step, which represents one of the most critical aspects in GB-InSAR, has been deeply discussed for each scenario.

The reliability of GB-SAR products has been demonstrated, representing an effective alternative for the design and implementation of prevention strategies, showing a high feasibility to hazard assessment and risk management.

Compared with PSI spaceborne solutions, GB-SAR sensors present several advantages due to the zero-baseline configuration of the instrument, which is firmly anchored on the same position for all acquisitions. The revisiting time is no longer a constraint due to the employment of a terrestrial platform. In addition, they offer the possibility to fit the illumination angle in order to maximize the detection of real ground displacement in the LOS direction. Anyway, this is strongly dependent on the characteristics of the site and in some cases it could not be possible. For instance, for urban subsidence monitoring not always there will be a nearby cliff. Finally, since APS may be perfectly estimated and compensated for, lower numbers of images are required in order to achieve reliable nonlinear estimations of the ground displacement processes. Compared with traditional in-field monitoring devices and techniques, including total stations, differential GPS, geological mapping, geophysical prospection, topographic leveling, extensometers, inclinometers, and piezometers, GB-SAR solutions have demonstrated to provide higher densities and to be very efficient in order to cover larger areas for long periods at lower cost.

Some future work lines may include the extension of the APS model-based techniques proposed in this paper for the monitoring of large-scale scenarios characterized by several kilometers in range. Moreover, the ability to solve unwrapping errors when facing more complex terrains and larger illuminated areas should be deeply analyzed.

ACKNOWLEDGMENT

The authors would like to thank Prof. J. Corominas and J. A. Gili from the Department of Geotechnical Engineering and Geosciences, Universitat Politècnica de Catalunya (UPC), their helpful discussions and support in the interpretation of the final displacement results over the test site of *El Forn de Canillo*. They also wish to thank the Institut Cartogràfic i Geològic de Catalunya (ICGC) for the ground-truth map provided in the test-site of *Sallent*, and finally, the firm Euroconsult for the inclinometric results for the test-site of *El Forn de Canillo*.

REFERENCES

[1] D. Massonnet and K. L. Feigl, "Radar interferometry and its application to changes in the Earth's surface," *Rev. Geophys.*, vol. 36, no. 4, p. 441, 1998.

[2] R. Bürgmann, P. A. Rosen, and E. J. Fielding, "Synthetic aperture radar interferometry to measure Earth's surface topography and its deformation," *Annu. Rev. Earth Planetary Sci.*, vol. 28, no. 1, pp. 169–209, May 2000.

[3] A. K. Gabriel, R. M. Goldstein, and H. A. Zebker, "Mapping small elevation changes over large areas: Differential radar interferometry," *J. Geophys. Res.*, vol. 94, no. B7, p. 9183, 1989.

[4] A. Ferretti, C. Prati, and F. Rocca, "Nonlinear subsidence rate estimation using permanent scatterers in differential SAR interferometry," *IEEE Trans. Geosci. Remote Sens.*, vol. 38, no. 5, pp. 2202–2212, Sep. 2000.

[5] A. Ferretti, C. Prati, and F. Rocca, "Permanent scatterers in SAR interferometry," *IEEE Trans. Geosci. Remote Sens.*, vol. 39, no. 1, pp. 8–20, Jan. 2001.

[6] O. Mora, J. J. Mallorqui, and J. Duro, "Generation of deformation maps at low resolution using differential interferometric SAR data," in *Proc. IEEE Int. Geosci. Remote Sens. Symp.*, 2002, vol. 5, pp. 2696–2698.

[7] P. Berardino, G. Fornaro, R. Lanari, and E. Sansosti, "A new algorithm for surface deformation monitoring based on small baseline differential SAR interferograms," *IEEE Trans. Geosci. Remote Sens.*, vol. 40, no. 11, pp. 2375–2383, Nov. 2002.

[8] O. Mora, J. Mallorqui, and A. Broquetas, "Linear and nonlinear terrain deformation maps from a reduced set of interferometric SAR images," *IEEE Trans. Geosci. Remote Sens.*, vol. 41, no. 10, pp. 2243–2253, Oct. 2003.

[9] C. Werner, U. Wegmuller, T. Strozzi, and A. Wiesmann, "Interferometric point target analysis for deformation mapping," in *Proc. IEEE Int. Geosci. Remote Sens. Symp. (IGARSS'03)*, 2003, vol. 7, pp. 4362–4364.

[10] A. Arnaud *et al.*, "ASAR ERS interferometric phase continuity," in *Proc. IEEE Int. Geosci. Remote Sens. Symp.*, 2003, vol. 2, pp. 1133–1135.

[11] A. Hooper, "A new method for measuring deformation on volcanoes and other natural terrains using InSAR persistent scatterers," *Geophys. Res. Lett.*, vol. 31, no. 23, p. L23611, 2004.

[12] R. Lanari *et al.*, "A small-baseline approach for investigating deformations on full-resolution differential SAR interferograms," *IEEE Trans. Geosci. Remote Sens.*, vol. 42, no. 7, pp. 1377–1386, Jul. 2004.

[13] A. Hooper, "A multi-temporal InSAR method incorporating both persistent scatterer and small baseline approaches," *Geophys. Res. Lett.*, vol. 35, no. 16, p. L16302, Aug. 2008.

[14] G. Fornaro, D. Reale, and F. Serafino, "Four-dimensional SAR imaging for height estimation and monitoring of single and double scatterers," *IEEE Trans. Geosci. Remote Sens.*, vol. 47, no. 1, pp. 224–237, Jan. 2009.

[15] A. Ferretti *et al.*, "A new algorithm for processing interferometric data-stacks: SqueeSAR," *IEEE Trans. Geosci. Remote Sens.*, vol. 49, no. 9, pp. 3460–3470, Sep. 2011.

[16] D. Tarchi *et al.*, "SAR interferometry for structural changes detection: A demonstration test on a DAM," in *Proc. IEEE Int. Geosci. Remote Sens. Symp. (IGARSS'99)*, 1999, vol. 3, pp. 1522–1524.

[17] H. Rudolf, D. Leva, D. Tarchi, and A. Sieber, "A mobile and versatile SAR system," in *Proc. IEEE Int. Geosci. Remote Sens. Symp. (IGARSS'99)*, 1999, vol. 1, pp. 592–594.

[18] D. Leva, G. Nico, D. Tarchi, J. Fortuny-Guasch, and A. Sieber, "Temporal analysis of a landslide by means of a ground-based SAR interferometer," *IEEE Trans. Geosci. Remote Sens.*, vol. 41, no. 4, pp. 745–752, Apr. 2003.

[19] S. Brown, S. Quegan, K. Morrison, J. Bennett, and G. Cookmartin, "High-resolution measurements of scattering in wheat canopies-implications for crop parameter retrieval," *IEEE Trans. Geosci. Remote Sens.*, vol. 41, no. 7, pp. 1602–1610, Jul. 2003.

[20] G. Nico, D. Leva, G. Antonello, and D. Tarchi, "Ground-based SAR interferometry for terrain mapping: Theory and sensitivity analysis," *IEEE Trans. Geosci. Remote Sens.*, vol. 42, no. 6, pp. 1344–1350, Jun. 2004.

[21] G. Luzi *et al.*, "Ground-based radar interferometry for landslides monitoring: atmospheric and instrumental decorrelation sources on experimental data," *IEEE Trans. Geosci. Remote Sens.*, vol. 42, no. 11, pp. 2454–2466, Nov. 2004.

[22] A. Aguasca, A. Broquetas, J. J. Mallorqui, and X. Fabregas, "A solid state L to X-band flexible ground-based SAR system for continuous monitoring applications," in *Proc. IEEE Int. Geosci. Remote Sens. Symp. (IGARSS'04)*, 2004, vol. 2, pp. 757–760.

[23] L. Pipia, A. Aguasca, X. Fabregas, and J. Mallorqui, "A polarimetric ground-based SAR system: First results at X-band," in *Proc. URSI Commiss. F Symp. Microw. Remote Sens. Earth Oceans Ice Atmos.*, Ispra, Italy, Jul. 2005.

[24] L. Noferini *et al.*, "Permanent scatterers analysis for atmospheric correction in ground-based SAR interferometry," *IEEE Trans. Geosci. Remote Sens.*, vol. 43, no. 7, pp. 1459–1471, Jul. 2005.

[25] M. Pieraccini, G. Luzi, and C. Atzeni, "Ground-based interferometric SAR for terrain elevation mapping," *Electron. Lett.*, vol. 36, no. 16, pp. 1416–1417, 2000.

[26] Z.-S. Zhou, W.-M. Boerner, and M. Sato, "Development of a ground-based polarimetric broadband SAR system for noninvasive ground-truth validation in vegetation monitoring," *IEEE Trans. Geosci. Remote Sens.*, vol. 42, no. 9, pp. 1803–1810, Sep. 2004.

[27] G. Bernardini, P. Ricci, and F. Coppi, "A ground based microwave interferometer with imaging capabilities for remote measurements of displacements," *Geotelematics Fair*, 2007.

[28] C. Werner, T. Strozzi, A. Wiesmann, and U. Wegmüller, "GAMMA's portable radar interferometer," *Proc. 13th FIG Symp. Deform. Meas. Anal.*, 2008, pp. 1–10.

[29] L. Pipia, "Polarimetric differential SAR interferometry with ground-based sensors," Ph.D. dissertation, Universitat Politècnica de Catalunya, Barcelona, Spain, 2009.

[30] K. Lukin and A. Mogyla, "Monitoring of St. Sophia Cathedral interior using Ka-band ground based noise waveform SAR," in *Proc. 6th Radar Conf., (EURAD'09)*, Rome, Italy, 2009, pp. 215–217.

[31] C. Del Ventisette *et al.*, "Using ground-based radar interferometry during emergency: The case of the A3 motorway (Calabria Region, Italy) threatened by a landslide," *Natural Hazards Earth Syst. Sci.*, vol. 11, no. 9, pp. 2483–2495, Sep. 2011.

[32] S. Rodelsperger, A. Coccia, D. Vicente, and A. Meta, "Introduction to the new metasensing ground-based SAR: Technical description and data analysis," in *Proc. IEEE Int. Geosci. Remote Sens. Symp.*, Jul. 2012, pp. 4790–4792.

[33] H. Lee, S. Member, J.-H. Lee, S. Member, and K.-E. Kim, "Development of a truck-mounted arc-scanning synthetic aperture radar," *IEEE Trans. Geosci. Remote Sens.*, vol. 52, no. 5, pp. 2773–2779, May 2014.

[34] N. Harries, D. Noon, H. Pritchett, and D. Bates, "Slope stability radar for managing rock fall risks in open cut mines," in *Proc. 3rd CANUS Rock Mech. Symp.*, Toronto, ON, Canada, May 2009, vol. 2009, pp. 1–8.

[35] D. Mecatti *et al.*, "Monitoring open-pit quarries by interferometric radar for safety purposes," in *Proc. 7th Eur. Radar Conf.*, Paris, France, Oct. 2010, pp. 37–40.

[36] P. Farina *et al.*, "IBIS-M: An innovative radar for monitoring slopes in open-pit mines," in *Proc. Int. Symp. Rock Slope Stabil. Open Pit Mining Civil Eng.*, Vancouver, BC, Canada, 2011.

[37] P. Farina and N. Coli, "Efficient real time stability monitoring of mine walls : The Çöllolar mine case study," in *Proc. Int. Mining Congr. Exhib. Turkey*, Antalya, Turkey, 2013, pp. 111–117.

[38] D. Tarchi *et al.*, "On the use of ground-based SAR interferometry for slope failure early warning: The Cortenova rock slide (Italy)," in *Landslides*, 2005, pp. 337–342.

[39] D. Tarchi, "Monitoring landslide displacements by using ground-based synthetic aperture radar interferometry: Application to the Ruinon landslide in the Italian Alps," *J. Geophys. Res.*, vol. 108, no. B8, p. 2387, 2003.

[40] N. Casagli, F. Catani, C. Del Ventisette, and G. Luzi, "Monitoring, prediction, and early warning using ground-based radar interferometry," *Landslides*, vol. 7, no. 3, pp. 291–301, May 2010.

[41] M. Pieraccini *et al.*, "Remote sensing of building structural displacements using a microwave interferometer with imaging capability," *NDT & E Int.*, vol. 37, no. 7, pp. 545–550, 2004.

[42] L. Pipia *et al.*, "Polarimetric differential SAR interferometry: First results with ground-based measurements," *IEEE Geosci. Remote Sens. Lett.*, vol. 6, no. 1, pp. 167–171, Jan. 2009.

[43] M. Crosetto, O. Monserrat, G. Luzi, M. Cuevas-González, and N. Devanthéry, "Discontinuous GBSAR deformation monitoring," *ISPRS J. Photogramm. Remote Sens.*, vol. 93, pp. 136–141, Jul. 2014.

[44] D. Tarchi, E. Ohlmer, and A. Sieber, "Monitoring of structural changes by radar interferometry," *Res. Nondestruct. Eval.*, vol. 9, no. 4, pp. 213–225, Jan. 1997.

[45] O. Montserrat, "Deformation measurement and monitoring with Ground-Based SAR," Ph.D. dissertation, Institute of Geomatics, Barcelona, Spain, 2012.

[46] L. Noferini, D. Mecatti, G. Macaluso, M. Pieraccini, and C. Atzeni, "Monitoring of Belvedere Glacier using a wide angle GB-SAR interferometer," *J. Appl. Geophys.*, vol. 68, no. 2, pp. 289–293, Jun. 2009.

[47] D. Tarchi, "Monitoring landslide displacements by using ground-based synthetic aperture radar interferometry: Application to the Ruinon landslide in the Italian Alps," *J. Geophys. Res.*, vol. 108, no. B8, p. 2387, 2003.

[48] G. Herrera *et al.*, "A landslide forecasting model using ground based SAR data: The Portalet case study," *Eng. Geol.*, vol. 105, no. 3–4, pp. 220–230, May 2009.

[49] G. Barla, F. Antolini, M. Barla, E. Mensi, and G. Piovano, "Monitoring of the Beauregard landslide (Aosta Valley, Italy) using advanced and conventional techniques," *Eng. Geol.*, vol. 116, no. 3–4, pp. 218–235, Nov. 2010.

[50] K. Takahashi, M. Matsumoto, and M. Sato, "Continuous observation of natural-disaster-affected areas using ground-based SAR interferometry," *IEEE J. Sel. Topics Appl. Earth Observ. Remote Sens.*, vol. 6, no. 3, pp. 1286–1294, Jun. 2013.

[51] O. Monserrat, M. Crosetto, and G. Luzi, "A review of ground-based SAR interferometry for deformation measurement," *ISPRS J. Photogramm. Remote Sens.*, vol. 93, pp. 40–48, Jul. 2014.

[52] R. Iglesias *et al.*, "Ground-based polarimetric SAR interferometry for the monitoring of Terrain displacement phenomena. Part I: Theoretical description," to be published.

[53] V. D. Navarro-Sanchez, J. M. Lopez-Sanchez, and L. Ferro-Famil, "Polarimetric approaches for persistent scatterers interferometry," *IEEE Trans. Geosci. Remote Sens.*, vol. 52, no. 3, pp. 1667–1676, Mar. 2014.

[54] R. Iglesias *et al.*, "Phase quality optimization in polarimetric differential SAR interferometry," *IEEE Trans. Geosci. Remote Sens.*, vol. 52, no. 5, pp. 2875–2888, May 2014.

[55] R. Iglesias *et al.*, "Polarimetric optimization of temporal sublook coherence for DInSAR applications," *IEEE Geosci. Remote Sens. Lett.*, vol. 12, no. 1, pp. 87–91, Jan. 2015.

[56] R. Hanssen, *Radar Interferometry: Data Interpretation and Error Analysis*. Norwell, MA, USA: Kluwer, 2001.

[57] J. Marturià, O. Mora, D. Xifre, P. Martínez, and A. Roca, "DInSAR techniques versus high topographic leveling surveys: The subsidence phenomena in Sallent," in *Proc. ECONGEO'06*, Barcelona, Spain, 2006.

[58] O. Mora, R. Arbiol, and V. Pala, "ICC's project for DInSAR terrain subsidence monitoring of the Catalonian territory," in *Proc. IEEE Int. Geosci. Remote Sens. Symp.*, 2007, pp. 4953–4956.

[59] L. Pipia, X. Fabregas, A. Aguasca, and C. Lopez-Martinez, "Atmospheric artifact compensation in ground-based DInSAR applications," *IEEE Geosci. Remote Sens. Lett.*, vol. 5, no. 1, pp. 88–92, Jan. 2008.

[60] R. Iglesias, "Atmospheric phase screen compensation in ground-based SAR with a multiple-regression model over mountainous regions," *IEEE Trans. Geosci. Remote Sens.*, vol. 52, no. 5, pp. 2436–2449, May 2014.

[61] L. Pipia, X. Fabregas, A. Aguasca, and C. Lopez-Martinez, "Polarimetric temporal analysis of urban environments with a ground-based SAR," *IEEE Trans. Geosci. Remote Sens.*, vol. 51, no. 4, pp. 2343–2360, Apr. 2013.

[62] R. Touzi, A. Lopes, J. Bruniquel, and P. Vachon, "Coherence estimation for SAR imagery," *IEEE Trans. Geosci. Remote Sens.*, vol. 37, no. 1, pp. 135–149, Jan. 1999.

[63] N. Santacana, "Estudi dels grans esllavissaments d'Andorra: Els casos del Forn i del vessant d'Encampadana." Ph.D. dissertation, Universitat Politècnica de Catalunya (UPC), Barcelona, Spain, 1994.

[64] I. Torrebadella *et al.*, "El Deslizamiento del Forn de Canillo en Andorra. Un Ejemplo de Gestión del Riesgo Geológico en Zonas Habitadas en Grandes Deslizamientos," in *Proc. 7th Simposio Nacional sobre Taludes y Laderas Inestables*, Barcelona, Spain, 2009, pp. 403–414.

[65] P. Blanco-Sánchez, J. J. Mallorquí, S. Duque, and D. Monells, "The Coherent Pixels Technique (CPT): An advanced DInSAR technique for nonlinear deformation monitoring," *Pure Appl. Geophys.*, vol. 165, no. 6, pp. 1167–1193, Aug. 2008.

Rubén Iglesias (S'12) was born in Barcelona, Spain, in 1982. He received the M.Sc. degree in telecommunication engineering from the Universitat Politècnica de Catalunya (UPC), Barcelona, Spain, in 2008. He is currently pursuing the Ph.D. degree from UPC, focused on the development of advanced differential synthetic aperture radar interferometry (DInSAR) and polarimetric DInSAR (PolDInSAR) techniques for the detection, monitoring, and characterization of slow-moving landslides with both orbital and ground-based SAR (GB-SAR) data.

From June 2009 to June 2010, he was with the Active Remote Sensing Unit, Institute of Geomatics, Barcelona, Spain, working in several projects related with the application of DInSAR to terrain-deformation monitoring with orbital and GB-SAR data. From June 2010 to March 2014, he was with the Signal Theory and Communications Department (TSC), UPC, working as a Research Assistant in the framework of DInSAR and GB-SAR DInSAR applications. In April 2014, he joined Altamira Information, an experienced Earth Observation Company in Barcelona dedicated to provide ground displacement measurements solutions by using DInSAR techniques.

Albert Aguasca (S'90–M'94) was born in Barcelona, Spain, in 1964. He received the M.Sc. and Ph.D. degrees in telecommunication engineering from the Universitat Politècnica de Catalunya (UPC), Barcelona, Spain, in 1989 and 1993, respectively.

Since 1995, he has been an Associate Professor with the School of Telecommunications Engineering, UPC. His teaching activities involve RF and microwave circuits for communications and radio navigation systems. He has published more than 40 papers on microwave synthetic aperture radar, radiometer systems, and microwave circuits. His research interests include the design and development of synthetic aperture radar and microwave radiometer systems for unmanned aerial vehicle (UAV) platforms.

Xavier Fabregas (S'89–M'93) received the B.S. degree in physics from Barcelona University, Barcelona, Spain, in 1988, and the Ph.D. degree in applied sciences from the Universitat Politècnica de Catalunya (UPC), Barcelona, Spain, in 1995.

In 1990, he joined the Photonic and Electromagnetic Engineering Group, Signal Theory and Communications Department, UPC. Since 1996, he has been an Associate Professor with the UPC. In 2001, he spent an eight-month sabbatical with the Microwaves and Radar Institute (HR), German Aerospace Agency (DLR), Oberpfaffenhofen, Germany. He has published 26 international journal papers and more than 106 conference proceedings and has received a patent. He is a Reviewer in several international journals. His research interests include polarimetric-retrieval algorithms, polarimetric calibration and speckle models, GB SAR sensors and their applications, and time series for multidimensional SAR data applications for urban and terrain deformation monitoring.

Jordi J. Mallorqui (S'93–M'96–SM'13) was born in Tarragona, Spain, in 1966. He received the Ingeniero and Doctor Ingeniero degrees in telecommunications engineering from the Universitat Politècnica de Catalunya (UPC), Barcelona, Spain, in 1990 and 1995, respectively.

Since 1993, he has been teaching with the School of Telecommunications Engineering of Barcelona, UPC, first as an Assistant Professor, later in 1997 as an Associate Professor, and since 2011 as a Full Professor. His teaching activity involves microwaves, radionavigation systems, and remote sensing. He spent a sabbatical year with the Jet Propulsion Laboratory, Pasadena, CA, USA, in 1999, working on interferometric airborne synthetic aperture radar (SAR) calibration algorithms. He is currently working on the application of SAR interferometry to terrain-deformation monitoring with orbital, airborne, and ground data; vessel detection and classification from SAR images; and 3-D electromagnetic (EM) simulation of SAR systems. He has published more than 100 papers on microwave tomography, EM numerical simulation, and SAR processing, interferometry, and differential interferometry in refereed journals and international symposia.

Dani Monells (S'11) was born in Sant Joan de les Abadesses, Spain, in 1981. He received the B.Sc. degree in telecommunication engineering from the Universitat Politècnica de Catalunya (UPC), Barcelona, Spain, in 2008. He is currently pursuing the Ph.D. degree focused on differential synthetic aperture radar interferometry (DInSAR) in orbital platforms, focusing on the exploitation of polarimetric SAR acquisitions (PolSAR), at the Signal Theory and Communications Department (TSC), UPC.

Since 2007, he has been working in several projects for the monitoring of terrain displacements and developing the TSC interferometric chain and processor, in order to give support to the new generation SAR satellites.

Carlos López-Martínez (S'97–M'04–SM'11) received the M.Sc. degree in electrical engineering and the Ph.D. degree from the Universitat Politècnica de Catalunya, Barcelona, Spain, in 1999 and 2003, respectively.

From October 2000 to March 2002, he was with the Frequency and Radar Systems Department (HR), German Aerospace Center (DLR), Oberpfaffenhofen, Germany. From June 2003 to December 2005, he has been with the Image and Remote Sensing Group, SAR Polarimetry Holography Interferometry Radargrammetry (SAPHIR) Team, Institute of Electronics and Telecommunications of Rennes (IETR), Rennes, France. In January 2006, he joined the Universitat Politècnica de Catalunya, Barcelona, Spain, as a Ramn-y-Cajal Researcher, where he is currently an Associate Professor in the area of remote sensing and microwave technology. His research interests include SAR and multidimensional SAR, radar polarimetry, physical parameter inversion, digital signal processing, estimation theory, and harmonic analysis.

Dr. López-Martínez is an Associate Editor of the IEEE JOURNAL OF SELECTED TOPICS IN APPLIED EARTH OBSERVATIONS AND REMOTE SENSING and he served as Guest Editor of the European Association for Signal Processing (EURASIP) Journal on Advances in Signal Processing. He has organized different invited sessions in international conferences on radar and SAR polarimetry. He has presented advanced courses and seminars on radar polarimetry to a wide range of organizations and events. He received the Student Prize Paper Award at the European Conference on Synthetic Aperture Radar (EUSAR) 2002 Conference and co-authored the paper awarded with the First Place Student Paper Award at the EUSAR 2012 Conference.

Luca Pipia received the B.S. degree (*cum laude*) in electrical engineering from the Università Degli Studi di Cagliari, Cagliari, Italy, in 2002, and the Ph.D. degree in polarimetric differential SAR interferometry (PolDIInSAR) from the Universitat Politècnica de Catalunya (UPC), Barcelona, Spain, in 2009.

From June 2001 to December 2001, he was with the High-Frequency Institute of the German Aerospace Center (DLR), Oberpfaffenhofen, Germany, where he worked on land classification using polarimetric SAR (PolSAR) information. From 2003 to 2009, he was with the Remote Sensing Laboratory, Departament de Teoria del Senyal i Comunicacions, UPC, where he was deeply involved in the development and assessment of a novel polarimetric formulation of coherence-based advanced DinSAR techniques using real ground-based PolSAR data. Currently, he is with the Remote Sensing Group, Institut Cartogrfic de Catalunya. His research interests include SAR polarimetry, differential SAR interferometry, and the retrieval of quantitative information from hyperspectral visible, near- and thermal-infrared airborne data.

Dr. Pipia has served as a Reviewer for the IEEE JOURNAL OF SELECTED TOPICS IN APPLIED EARTH OBSERVATIONS AND REMOTE SENSING, the IEEE GEOSCIENCE AND REMOTE SENSING LETTERS, and the IEEE TRANSACTIONS ON GEOSCIENCE AND REMOTE SENSING.